Horvath, K.; Drozdenko, D.; Mathis, K.; Bohlen, J.; Dobron, P.:

Deformation behavior and acoustic emission response on uniaxial compression of extruded rectangular profile of Mg- Zn-Zr alloy

In: Journal of Alloys and Compounds (2016) Elsevier

DOI: 10.1016/j.jallcom.2016.03.310

Deformation behavior and acoustic emission response on uniaxial compression of extruded rectangular profile of Mg-Zn-Zr alloy

Klaudia Horváth[a], Daria Drozdenko[a], Kristián Máthis[a], Jan Bohlen[b], Patrik Dobroň[a]

[a]Charles University in Prague, Department of Physics of Materials, Ke Karlovu 5, 121 16, Prague 2, Czech Republic

[b]Helmholtz-Zentrum Geesthacht, MagIC – Magnesium Innovation Centre, Max Planck Str. 1, Geesthacht D21502, Germany

Abstract

The mechanical behavior of Mg-Zn-Zr alloy in a form of extruded rectangular profile is related to the initial crystallographic texture and the twinning activity. The profile with a thickness of 10 mm was uniaxially compressed in three directions (extrusion (ED), transversal (TD) and normal direction (ND)) at room temperature. Concurrently, acoustic emission (AE) measurements were performed in order to study the deformation mechanisms. The AE events, stemmed from collective dislocation movement and the twin nucleation, were identified using statistical analysis of the raw AE signal. The texture evolution was studied by X-ray diffraction on samples deformed in compression up to a specific stress levels. Along the ED and TD the dominant deformation mechanism is extension twinning, which is accompanied by intensive acoustic emission and strain hardening increment. In contrast, dislocation slip prevails in ND, which causes deformation curves similar to that usually observed in tension.

Keywords

Extruded profiles, texture development, acoustic emission, clustering, work hardening

1. Introduction

Recently, the demand for wrought magnesium alloys as light-weight construction materials has been raised in many technical applications owing to their propitious strength-to-weight ratio. Generally, the forming (extrusion, rolling etc.) process improves the mechanical properties of Mg alloys compared to cast alloys [1, 2]. At the same, the extruded Mg alloys usually exhibit pronounced textures with basal planes orientated nearly parallel to the extrusion direction (ED). Such a texture favors $\{10\bar{1}2\}\langle 10\bar{1}1\rangle$ twinning during compression along the ED or transversal direction (TD). The activation of twinning results in lower yield strength (YS) in compression than in tension [3]. Since such a tension-compression asymmetry (TCA) of the YS represents significant limitation for industrial applications, the methods for its reduction are intensively investigated [4, 5]. Texture weakening achieved by proper addition of alloying elements has been found as the most effective way for TCA reduction [6]. The modification of the texture leads to changes in mechanical properties. Thus, the investigation of the dependence of the deformation mechanisms on the loading mode and the initial texture is of key importance. Weaker texture can reduce the TCA, however also leads to lower values of the YS [7].

Diffraction methods belong to the most important experimental techniques, which give information about the microstructure evolution from a statistically relevant volume. Recently, several papers have been published in this topic, which are focused on twinning evolution as a function of the loading mode [8 - 10] in dependence of the texture evolution on the mutual orientation of the extrusion and loading direction [11, 12].

Besides diffraction techniques, acoustic emission (AE) has been found as a powerful non-destructive technique for study of deformation mechanisms. This *in-situ* method gives integral information from entire volume about the dynamic processes during plastic deformation. Despite the generally different character of a dislocation and a twinning signal (continuous vs. burst), making difference between them is a difficult task owing to the concurrent activity of both. There are several statistical methods for separating the signals from different sources [13 - 17]. In our work we applied the recently published algorithm of Pomponi and Vinogradov [18], which allows to determine the dominant deformation mechanism in a given time period by means of processing the raw (not filtered) AE signal.

The main goal of the present work is to find a link between the initial texture of the material and the deformation behavior in compression. The rectangular profile used in this study as the

initial material allows different textures in the three sample orientations (ED, TD, ND) to be realized. The novelty consists also in the proper combination of *in-situ* and *post-mortem* methods, as AE and X-ray for investigation of the activity of various deformation mechanisms.

2. Materials and methods

Gravity cast ZK10 (Mg + 0.9 wt. % Zn + 0.1 wt. % Zr) magnesium alloy was extruded at 250 °C with an extrusion speed of 10 mm/s (profile exit speed) through a rectangular section of dimensions 100 x 12 mm into the final form.

The deformation tests were carried out on a universal testing machine INSTRON® 5882 at room temperature (RT) with a constant strain rate of 10^{-3} s^{-1}. The samples of (10 x 10 x 10) mm^3 were compressed along three directions: ED, TD and ND. The compression tests were repeated and stopped at specific stress values in order to follow a development of the texture during loading.

The AE during deformation tests was monitored by a computer-controlled system MICRO-II developed by Physical Acoustic Corporation (PAC), which allows a continuous storage of AE signals with a sampling frequency of 1 MHz. A piezoelectric sensor MIDI-410-61 (ZD RPETY-DAKEL) with a diameter of 6 mm was used. The AE sensor was attached on the sample with a help of a clamp. Vacuum grease was used in order to improve the contact between the sample and the AE sensor. High signal/noise ratio was ensured using a 40 dB preamplifier. A threshold-level detection of the recorded AE signals was also performed to achieve a comprehensive set of AE parameters. The threshold level was set to 26 dB.

For microscopic observations, the samples were grinded on SiC papers and subsequently polished by diamond pastes down to 0.25 μm particle size. The polished surfaces were etched first in 5 % Nital for 5 s and then in solution of 50 ml ethanol, 9 ml water, 4 ml acetic acid and 6 g picric acid for 10 s. The microstructure of the Mg alloy was investigated in ED-TD plane by OLYMPUS GX51 microscope equipped with the PIXELINE® camera.

Texture measurements were performed on polished samples (perpendicular to the ED) using an X-ray diffraction machine with goniometer table of PANalytical using CuK_α radiation. A computer code MTEX [19] was applied to calculate the orientation distribution function and recalculate full pole figures in the ED-TD plane.

3. Results

The microstructure and initial texture of the ZK10 magnesium alloy are presented in Fig. 1. The investigated alloy exhibits an inhomogeneous microstructure. The average grain size evaluated using the ASTM E1181 standard was (16.86±5.54) μm in fine grained and (38.55±6) μm in coarse grained part, respectively. A strong texture with basal planes perpendicular to the ND with slight tilt to the TD was observed. In the (10-10) pole figure, the prismatic planes appear in a six-peak alignment.

3.1 Mechanical properties

Mechanical properties of extruded ZK10 alloy compressed along various axes are listed in Table 1.

Mg alloy	Sample orientation	CYS (MPa)	UCS (MPa)	Uniform elongation (%)	Fracture strain (%)
ZK10	ED	54 (±2)	293 (±2)	8.5 (±0.3)	8.8 (±0.3)
	TD	52 (±3)	252 (±2)	4.6 (±0.3)	5.1 (±0.3)
	ND	120 (±5)	259 (±2)	5.8 (±0.3)	9.0 (±0.3)

Table 1 Mechanical properties of extruded ZK10 magnesium alloy deformed along various axes; CYS – compressive yield strength, UCS – ultimate compressive stress.

It is obvious that the CYS for loading along the ED and TD are comparable, whereas in ND direction its value is doubled.

The true stress, strain hardening rate and the AE count rate[1] vs. true strain curves for the ED, TD and ND samples are presented in Fig. 2. The deformation curves for the ED and TD sample have a characteristic S-shape, whereas the ND sample exhibit convex shape, typical rather for tensile tests.

The strain hardening rate curves for the ED and TD samples show an apparent lift above 3% of strain, which corresponds to the inflection point on the deformation curve. This lift is more pronounced for the TD than for ED sample. For the ND sample, the strain hardening rate decreases monotonically from the yield point towards the end of the test. It is worth to note that the AE count rate drops to zero close to the above mentioned inflection point for ED and

[1] The AE count rate is a parameter, which determines the number of the emitted pulses with amplitude greater than the threshold level per a time unit [20] – in our case per second.

TD sample orientations. Further, its peak value is significantly smaller for the ND sample than that for the other two samples.

3.2 Texture evolution

In order to study the effect of the ongoing deformation as a result of active slip systems and especially twinning, besides AE measurement, the texture analysis by X-ray diffraction was performed on the samples, which were compressed up to specific stresses (hereafter denoted as position 1-5 and labeled in Fig. 2, Table 2). The results of texture measurements are presented in Figs. 3-5.

	ED		TD		ND	
	Stress	Remark	Stress	Remark	Stress	Remark
Position 1	70	after the yield point	75	after the yield point	140	after the yield point
Position 2	75	minimum of hardening rate	85	minimum of hardening rate	220	ongoing deformation
Position 3	100	after the disappearance AE signal	130	after the disappearance AE signal		
Position 4	200	maximum of hardening rate (inflection point)	190	maximum of hardening rate (inflection point)		
Position 5	250	after the inflection point				

Table 2 Remarks for the texture measurements

As it is mentioned above, the ZK10 magnesium alloy exhibits texture with basal planes oriented perpendicular to the ND (Fig. 3a). A small angular spread of basal planes towards the TD is observed.

For the ED sample deformed up to the yield point (Fig. 3b), the peak intensity in the basal (0001) pole figure is higher than that for the as extruded sample. After compression up to 75 MPa (Fig. 3c) two components in the (0001) pole figure towards the ED can be seen. The intensity of these two components increases with increasing plastic deformation (Fig. 3d-f). In other words, during compression along the ED the basal planes have been moved from the ND to ED (Fig. 3f).

Compression loading along the TD leads to the formation of two components towards the TD (Fig. 4b). As deformation proceeds, the intensity of these components becomes stronger (Fig. 4c-e). After compression up to 190 MPa, the basal planes are tilted toward the TD (Fig. 4e).

During compression along the ND, no significant changes in the crystallographic texture are observed (Fig. 5). The basal planes remain perpendicular to the ND till the end of the test and the peak intensity of this texture increases with increasing plastic deformation.

3.3. Clustering of the AE signal

Raw AE signals recorded during compression tests were further analyzed using the adaptive sequential k-means (ASK) procedure. The clustering procedure, worked out by Pomponi and Vinogradov, is described in detail in Ref. [18]. A brief overview about the main steps is given here:

- The recorded waveform streaming data are sectioned into consecutive frames. In our case the sampling frequency was 1 MHz, and the frame size was set as 2048 samples. Thus a single frame corresponds to a 2 ms long "*time window*".
- After the Fast Fourier Transformation (FFT) of the signal, the Power spectral density (PSD) function is calculated for each frame.
- The features of the PSD in the first frame define Cluster 1.
- PSDs in the consecutive frames are analyzed one-by-one. If the statistical properties of a given PSD are similar to those in an already existing cluster, this PSD is assigned to this cluster. If not, a new cluster is established. The conditions for new cluster forming are based on *k*-means method.

When the clustering procedure is completed, a dominant AE source mechanism is assigned to each cluster. This assignment consists of three basic steps:

1. Checking the time of the appearance of the elements in a given cluster. For example, since the recording of AE data is always launched *before* the starting of the deformation test, the elements in Cluster 1 naturally belong to the background noise.
2. Checking characteristic features of the PSDs, as energy, frequency distribution etc. For example, the twin nucleation usually emits AE signal with larger energy than that of dislocations.
3. Comparison of the results with the supplementary data, as texture measurement, microscopy, theoretical modeling etc.

Finally, the increment of the number of elements with time (Cumulative Number of Elements) can be plotted. Such a graph characterizes the dynamics of the deformation mechanisms.
Based on the above mentioned algorithm, the particular clusters formed by the ASK algorithm during analysis of our signals can be identified as follows:

- Cluster 1 – BACKGROUND NOISE (color code in figures – black)
  a) The AE signals in frames before the launching of the deformation test belong to this cluster.
  b) They are typically low energy signals – see Fig. 7a-c (Energy vs. Median Frequency plot[2]).
  c) The related number of events increases before the beginning of the test. Events are not detected during the test in the range where events from other clusters are identified because they are not dominating the AE signal in this part of the experiment. After the activity of the other clusters comes to an end, this cluster is the only detectable once again and the number of events increases.
- Cluster 2 – BASAL SLIP (color code in figures – blue)
  a) The basal dislocation-type AE events usually exhibit a continuous character [21, 22] (cf. Fig. 6a), which is a convolution of small burst signals originated from dislocation avalanches [23]. A cluster with AE events of medium energy will result from Ref. [24]. The large energy signals are most probably emitted by densely populated dislocation avalanches at the beginning of the straining. As the deformation progress, the energy decreases and the frequency range increases as a consequence of decreasing mean free path for dislocation movement.
  b) The number of events in this cluster starts to increase somewhat at the beginning of the deformation, at low applied stresses (Fig. 8-9). It is visible in all three experiments to a distinct extent. This behavior is in good agreement with basal slip, which has the lowest critical resolved shear stress (CRSS) [25] among the deformation mechanisms in Mg and therefore will be active preferentially in typical wrought materials even if the texture is strong [see e.g. 26, 27].

- Cluster 3 – TWINNING NUCLEATION (color code in figures – green)
  a) This cluster refers to events with high median frequency and high energy. It consists of signals of burst type (Fig. 6b) which is consistent with the nature of

[2] The overlapping of the clusters is given by 2D projection of a multidimensional space. From the statistical point of view the clusters are well separated.

twin nucleation [28]. It is worth mentioning at this point that twin growth will not cause AE and is therefore not visible in the AE signal as well as in the corresponding cluster identified here.

b) Also this cluster appears at the early stage of straining. Such a feature has been observed also by other authors [29, 30], and indicates the onset of nucleation of $\{10\bar{1}2\}\langle 10\bar{1}1\rangle$ twins.

- Cluster 4 – NON-BASAL SLIP (color code in figures – red)
  a) The average energy level of the signals is lower compared to cluster 2 (basal slip). It also includes events of continuous signal character. A review of the results in Fig. 7 a-c reveals that this cluster is visible from the very beginning of the test. A mechanism resulting in events with lower energy, e.g. because of less distinct avalanches of dislocations, is easily correlated to a harder to activate slip mechanism. The wide frequency distribution is also characteristic for dislocation-origin signals [24].
  b) Theoretical models, as e.g. EPSC model [27] predict activity of non-basal slip at the early stage of deformation. In delimitation to cluster 2 (basal slip) this cluster can therefore be assigned to non-basal slip. So far, the ASK algorithm cannot make a difference between particular non-basal slip types (prismatic or pyramidal <*a*>-slip, <*c*+*a*>-slip). This is also consistent with the fact that CRSS for non-basal slip systems (although also varying) are distinctly higher than that for basal slip [31]. For the purpose of separating the respective non-basal slip systems and their activity, diffraction experiments can be used [24, 32].
  c) It has been discussed [24] that the reason for lower energy can be a reduced mean free path of non-basal dislocations, which have to overcome dislocation-type obstacles. This is found in materials with non-preferable activation of non-basal slip.

Fig. 7 collects the dependence of two parameters as results of the ASK, energy and median frequency, plotted for the three compression experiments of this work. In all three cases different preferential ranges can be revealed for different clusters. Cluster 1 (black), associated with noise signals, is found in all three cases at low energies at medium median frequency. Cluster 2 (blue), associated with basal slip, is found at medium energies in a wide range of median frequencies. It is significant that in case of ND compression the cluster is

shifted to a range of higher median frequencies. Cluster 3 (green), associated with twinning, collect events with higher energies and high median frequencies. It is clearly visible that the median frequency range of this cluster decreases from the ED compression test to the TD compression test and even more to the ND compression test. In case of the ND compression test the number of events is very low compared to the two other directions. Cluster 4 (red), associated with non-basal slip, is clearly visible at lower energies and medium median frequencies. Still, the average median frequency is higher compared to cluster 2 (basal slip) in case of the ED and TD compression tests whereas, vice versa, it is lower or similar compared to cluster 2 in case of the ND compression test. In summary, the different clusters, associated with some specific deformation mechanisms, are clearly distinguished in the energy-median frequency plots and show some distinct differences if the compression direction is changed.
It is worthwhile to repeat that the ASK algorithm includes more parameters than only the energy and the median frequency during analysis to separate different events and assign them to different clusters. Therefore, by restricting the presentation of the analyzed signal in this work to the two properties energy and median frequency, results in an overlap of the ranges in the plots for different clusters.

Fig. 8 a-c show the time evolution of the cumulative number of events of different clusters for the three compression experiments in ED, TD and ND. Fig. 9 a-c show the same for the cumulative energy. Thus, the first plots sum up the number of events vs. time as they occur in the clusters and the second plots sum up their respective energies vs. time.

There is a significant difference between the time evolutions of the particular clusters. Cluster 1 (noise) naturally occurs first in all three experiments as the number of events as well as cumulative energy start to increase even before the start of the test. During the test, if signals of other source mechanism dominate the assignment of the respective events to other clusters, the number and cumulative energy of the noise cluster remains constant. It only starts to increase again at a time when no other signals from the material could be assigned to other clusters any more. This is the case at times in the experiments where the AE count rates (see Fig. 2) are already very low. This finding underlines that the signal of the respective mechanism dominates the assignment to a specific cluster. Vice versa, it does not mean that the mechanisms that do not dominate the AE signals are not active. They, at this moment, do not dominate the signal.

At the onset of straining, the cluster of non-basal slip dominates the AE signal in all three cases. Thus, there is a certain increase in the number of this cluster which ends the increase of the noise cluster. The number of events is quite low at this point.

With the further increase of strain, the development in the three compression tests is different. In case of ED compression (Fig. 8a) an increase of the number of events in cluster 2 (basal slip) is found, which grows to a maximum value. This is followed by a distinct increase of the number of twin event (cluster 3) around the yield point. With proceeding plastic deformation, after the number of events in cluster 3 is saturated, the number of events in cluster 4 (non-basal) starts to increase further.

During TD compression (Fig. 8b) higher number of events is found in the cluster 2 (basal) before cluster 4 again dominates the signal. This is followed by a distinct increase of the number of twin event (cluster 3), which increases later than in case of ED compression. The increase of this cluster (twinning) takes places along with the yield point. The number of events in cluster 3 during TD compression is lower compared to ED compression. With proceeding plastic deformation, after stabilization of the number of events in cluster 3, the number of events in cluster 4 (non-basal) starts to increase further.

In case of ND compression (Fig. 8c) the situation is different. After the onset of the increasing event numbers of cluster 2 there is a concurrent increase of both, the number of events of cluster 2 and 4. Thus, signals related to basal slip and non-basal slip are visible in the same time frame and the AE signal is not only dominated by one specific cluster. Furthermore, cluster 3 (twin nucleation) only shows a small number of events occurring at a later time – not necessarily related to the yield point - and also concurrent to signal of the slip related clusters 2 and 4. Moreover, number of events in cluster 4 (non-basal) continues to increase after the saturation of number of events in cluster 2 (basal).

The common feature of twinning events is that for all directions the number of elements does not increase above a certain level of strain. This feature can be substantiated by the fact that the AE method is sensitive only on the twin nucleation, in which a large number of twin dislocations are involved [33, 34]. The twin growth (i.e. its increment in thickness) cannot be detected owing to slow motion of the twin boundary, which causes only low energy elastic waves [35]. Finally, the results indicate that the twin nucleation is most significant in ED and slightly less significant in TD, whereas in ND the role of twinning is minor.

Qualitatively, the development of the cumulative energies of different clusters is essentially the same as in case of the number of events. This is easily understood because each event will contribute with its energy. However, the level of the cumulative energy can help to reveal

which deformation mechanism gives a higher impact to the deformation than others. As we can see in TD compression a relative lower number of events compared to ED compression leads to a higher cumulative energy of this cluster which indicated the higher impact of twin nucleation in TD compared to ED. Concurrent to this it can be seen in Fig. 7a-b that in the case of TD compression cluster 3 (twinning) is more concentrated at higher median frequency compared to ED compression.

In case of ND compression twin nucleation obviously has a neglectable impact on the deformation. Cluster 2 and 4 dominate the events. If looking at the events of cluster 2 (basal slip) a comparable number of events in ND compression as in TD compression lead to a lower cumulative energy in ND. In Fig. 7 it can be seen that this is because in ND compression there are no signals at lower median frequency and higher energy. Thus, direct comparison of the cumulative energies in cases where different deformation mechanisms dominate may be misleading. In summary of the ND compression test the concentration of cluster 2 at higher median frequencies requires some attention during the discussion of the results.

4. Discussion

The rectangular shape of the extruded profile in this study allows a conclusion on the direction dependence of the mechanical properties because of varied activity of different deformation mechanisms, which has a link to the distinct texture of this material. A strong alignment of basal planes with the c-axis parallel to ND is combined with a broad tilt towards TD as well as a distinct angular distribution of basal planes towards ED at high intensities. Grains with c-axes parallel to TD can be found, but not parallel to ED. The prismatic pole figure is also distinct with 6 clearly visible peaks which indicate that the material is not fully recrystallized but still contains remains of unrecrystallized grains [35]. Even if the material does not appear in a fully recrystallized condition, the microstructure consists of equi-axed grains of broad grain size distribution without clearly visible fraction of grains with shape orientation. Therefore, the resulting anisotropic properties will not be dependent on the grain shape but distinctly related to the texture of the samples.

The obvious lower CYS measured in ED and TD correlates with a distinct work hardening behavior which has been associated with a preferential activation of twinning [36]. There is no visible difference in the CYS comparing ED and TD compression although the two compression samples have a clearly different texture with respect to the loading axis. The

work hardening behavior is different, being more pronounced in TD compression than in ED compression. In case of ND compression, the CYS is much higher and with the work hardening behavior it can be concluded that twinning does not play a major role in both, yielding and work hardening.

4.1 The ED compression test

The texture development during compression along ED shows that re-orientation due to twins started in the beginning of the test. Without addressing the results from the cluster analysis at this point the fact that AE is high motivates that the underlying mechanism is twin nucleation. After a while, AE drops to zero but the texture change continues up to the inflection point of the curve. This is well understood by the fact that twin nucleation is a source of AE whereas twin growth is not [33]. Thus, the nucleation of new twins with increasing strain decreases during work hardening far before the inflection point. Twin growth is then favored over the nucleation of new twins.

The ASK analysis favors twin nucleation as the mechanism taking control at the yield point. In the range before the yield point is reached there is some activity identified as non-basal as well as basal slip. That basal slip is more pronounced in this case is consistent with earlier findings in materials with distinct textures.

As twin nucleation comes to an end – which is even earlier than the full drop of AE and specifically at the beginning of the decrease of the AE count rate from its peak value, cluster 4 (non-basal slip) grows to some significance. In this strain range re-orientation of basal planes continues due to twin growth into an orientation where basal slip will not contribute to strain accommodation anymore.

4.2 *The TD compression test*

The results obtained from TD compression have a clear similarity to those obtained in ED compression but also show some distinct differences. The work hardening during the test is higher, the hardening rate grows to a higher peak level and the test ends earlier, i.e. the fracture strain is lower. Corresponding to this, the AE count rate decreases faster compared to ED. The related texture in position 2 (Fig. 4c) is already quite strong (7.0 m.r.d.) based on a twin related re-orientation of the grains. It is even stronger than the texture in position 3 (5.0 m.r.d.) for ED compression (Fig. 3d). The ASK analysis of the TD compression test shows that twin nucleation is going faster compared to ED during the test. This is also visible in the

higher cumulative energy of this mechanism in TD compared to ED which reveals its higher impact on the hardening process.

Twinning will form a texture component with c-axis parallel to the compression axis. In case of ED compression, basically all grains have orientations in favor of twinning which can re-orient. In case of TD compression this is not the case, although still a higher fraction of grains is favorable oriented for twinning. Some grains with tilt of the c-axis towards TD or even parallel to TD have it harder to reorient or are not in favor for this at all. This explains well why the number of twin nucleation events is lower than in ED. It furthermore requires that the lower number of grains favorably oriented for twinning still contribute to strain accommodation in a comparable way as in ED. Such a driving force for twin nucleation should then have an impact on the energy of a twin nucleation event as identified in cluster 3 of the TD measurement. Then the twins will also grow faster which is consistent with the finding in the texture measurements.

The end of twin nucleation corresponds to the end of a distinct drop in the AE count rate, which is followed by a less significant decrease. Thus, there is a visible transition in the count rate curve from twin nucleation to non-basal slip.

Regarding cluster 2 (basal slip) the higher number of events in the beginning of TD compression compared to ED compression indicates a higher activity of basal slip, which is consistent with the texture of the material, i.e. some grains are favorably oriented for basal slip in TD compression whereas they are not in ED compression.

From ASK it is also seen that non-basal slip is active already before twin nucleation and then again active when cluster 4 does not have further impact. Especially the first increase of the non-basal slip cluster is not seen in case of ED compression but is quite distinct in case of TD compression. The delayed increase of events in cluster 3 (twin nucleation) obviously reveals active slip on non-basal planes which is expected. Owing to the less intensive twinning, the extent of non-basal <a> slip is larger than that in the ED direction. Thus, the component of the non-basal <a> slip prevails in the PSD spectrum around the yield point. Thus, the visibility of this cluster is not surprising but it indicates the lower impact of twin nucleation because of the different dominance of clusters in TD compression compared to ED compression.

The curve of the non-basal slip cluster 4 later has another increase in case of both, ED and TD compression. Thus, non-basal slip becomes visible again after twin nucleation and basal slip came to the end. In order to read this result properly it can be concluded that non-basal slip appears as the only detectable mechanism because twin nucleation came to an end and basal

slip is not visible any more due to some distinct work hardening. This requires that such work hardening is not that significantly extended to the non-basal slip systems.

4.3 The ND compression test

From the texture analysis it is obvious that there are only few grains with c-axis parallel to TD that will preferentially twin. The strengthening of the texture with a main component in ND during ND compression is more indicative for slip rather than twinning, because reorientation of grains with c-axis parallel to TD towards ND the texture change is only gradual. Since twinning is not favorable, strain can be accommodated by non-basal slip, e.g. <c+a> slip. This is consistent with the higher number of events in cluster 4 (non-basal) in ND compression compared to the other two directions. However, the increase in the number of events in cluster 4 is accompanied by an increase in the number of events in cluster 2 (basal slip).

Thus, a concurrent activation of basal as well as non-basal slip both determine the cluster assignment of the signals. In this orientation an interaction of different types of dislocations is conclusive. Thus, a development of obstacles due to dislocation interaction is consistent with events of higher median frequency [24]. This explains well the concentration of events in cluster 2 (basal) at higher median frequencies and medium energy. Moreover, such an effect is not distinct in case of non-basal slip (cluster 4). This is also consistent with the approach that non-basal slip is harder to activate, e.g. because of a higher CRSS and will not be strain hardened that significantly.

Conclusions

An extruded profile of alloy ZK10 alloy is used in this work to carry out compression tests in different orientations in order to investigate the texture effect on the mechanical properties as well as the related deformation mechanisms. For this purpose, texture analyses at specific pre-strains related to the tests have been used in an ex-situ approach as well as in-situ AE measurement and a related ASK analysis in order to reveal the dominant mechanisms. At the same time such experiments are used to validate the results of the ASK analysis.

The compressive yield stress and the related work hardening behavior are indicative for preferential twinning in ED and TD compression. It is revealed that in TD compression a lower number of grains is favorable oriented for twinning than in ED compression. This results in a lower number of twins which have a higher impact as revealed from the energy of the respective cluster as well as the more pronounced work hardening. In case of ND

compression twinning plays a minor role. It is also not preferentially active as seen from the ASK analysis as well as from the gradual change of the texture. The slip dominated plastic deformation consists of interaction of basal and non-basal slip which a higher tendency to work hardening for basal slip.

The ASK analysis exhibits the dominant mechanism active in the respective stage of the experiment carried out. The energy and the median frequency as two important parameters of the cluster analysis (neglecting the importance of the other parameters that contribute to the clear identification of the clusters) allow conclusions to be drawn on the preferential activity of deformation mechanisms.

Moreover, the parameter range of events of different clusters is related to the impact of the mechanisms, characterized by their respective ranges of energies and, e.g. with respect to work hardening, median frequencies.

The formation of obstacles during straining or the free movement of dislocation as dislocation avalanches are related to differences in the parameter range of AE events in different clusters.

Acknowledgement

This work was completed within the framework of the research grant 13 - 19812S by the Czech Science Foundation (PD, JB), the grant SVV-2015-260217(KH), SVV-2015- 260213 and the Grant Agency of Charles University under the grant 1882314 (DD).

References

[1] M. Avedesian, H. Baker, *ASM Specialty Handbook Magnesium and Magnesium Alloys, ASM International, Materials Park, OH (1999).*

[2] C.J. Bettles, M.A. Gibson, *JOM 5 (2005) 46 - 49*.

[3] D.L. Yin, J.T. Wang, J.Q. Liu, X. Zhao, *J Alloys Compd. 478 (2009) 789–795.*

[4] J. Jain, W.J. Poole, C.W. Sinclair, M.A. Gharghouri, *Scr. Mater. 62 (2010) 301-304.*

[5] C. Lv, T. Liu, D. Liu, S. Jing, W. Zeng, *Mater. Des. 33 (2012) 529-533.*

[6] J. Bohlen, M. R. Nürnberg, J. W. Senn, D. Leityig, S. R. Agnew, *Acta Mater. 55 (2007) 2101-2112.*

[7] K. Illkova, P. Dobroň, F. Chmelík, K. U. Kainer, J. Balík, S. Yi, D. Letzig, J. Bohlen, *J Alloys Compd. 617 (2014) 253-264.*

[8] J. Čapek, K. Máthis, B. Clausen, J. Stráská, P. Beran, P. Lukáš, *Mater. Sci. Eng. A 602 (2014) 25-32.*

[9] O. Muránsky, D.G. Carr, P. Šittner, E.C. Oliver, *Int. J. Plast. 25 (2009) 1107-1127.*

[10] B. Clausen, C.N. Tomé, D.W. Brown, S.R. Agnew, *Acta Mater. 56 (2008) 2456-2468.*

[11] D. Sarker, J. Friedman, D.L. Chen, *J. Mater. Sci. Technol. 31 (2015) 264-268.*

[12] M.R. Barnett, Z. Keshavarz, A.G. Beer, D. Atwell, *Acta Materialia 52 (2004) 5093–5103*

[13] A. Kontsos, T. Loutas, V. Kostopoulos, K. Hazeli, B. Anasori, M.W. Barsoum, *Acta Mater. 59 (14) (2011) 5716-5727.*

[14] Y.P. Li, M. Enoki, *Mater. Sci. Eng. A 536 (2012) 8-13.*

[15] J. Jiao, C. He, B. Wu, R. Fei, X. Wang, *Int. J. Press. Vessel. Pip. 81 (2004) 427-431.*

[16] E.P. Sereano, M.A. Fabio, *IEEE Trans. Signal Process. 44 (1996) 1270-1275.*

[17] M.A. Hamstad, A. O´Gallagher, J. Gary, *J. Acoust. Emiss. 20 (2002) 39-61.*

[18] E. Pomponi, A. Vinogradov, *Mech. Syst. Signal Process. 40 (2013) 791-804.*

[19] F. Bachmann, R. Hielscher, H. Schaeben , *Solid State Phenom. 160 (2010) 63-68.*

[20] Acoustic Emission Standard Terminology ASTM E1316-05

[21] A. Vinogradov, A. Lazarev, *Scr. Mater. 50 (2012) 777-781.*

[22] D. Drozdenko, J. Bohlen, F. Chmelík, P. Lukáč, P. Dobroň, *Mater. Sci. Eng. A 650 (2016) 20-27.*

[23] C.R. Heiple, S.H. Carpenter, *J. Acoust. Em. 6 (1987a) 177-204.*

[24] K. Máthis, G. Csiszár, J. Čapek, J. Gubicza, B. Clausen, P. Lukáš, A. Vinogradov, S.R. Agnew, *Int. J. Plast. 72 (2015) 127-150.*

[25] A. Akhtar, E. Teghtsoonian, *J. Min. Met. Mat. S20 (1968) A73-A79.*

[26] S.R. Agnew, O. Duygulu, *Int. J. Plast. 21 (2005) 1161-1193.*

[27] S.B. Yi, CH.J. Davies, H.G. Brockmeier, R.E. Bolmaro, K.U. Kainer. J. Homeyer, *Acta Mater. 54 (2006) 549-562.*

[28] J.P. Toronchuk, *Mater. Eval. 35 (1977) 51-53.*

[29] A. Vinogradov, A. Lazarev, M. Linderov, A. Weidner, H. Biermann, *Acta Mater. 61 (2013a) 2434-2449.*

[30] A. Vinogradov, D. Orlov, A. Danyuk, Y. Estrin, *Acta Mater. 61 (2013b) 2044-2056.*

[31] A. Staroselsky, L. Anand, *Int. J. Plasticity 19 (10) (2003) 1843-1864.*

[32] K. Máthis, K. Nyilas, A. Axt, I. Dragomír-Cermatescu, T. Ungár, P. Lukáč, *Acta Mater. 52 (2004) 2889-2894.*

[33] V.M. Finkel, I.N. Voronov, A.M. Savelyev, A.I. Yeliseyev, V.A. Fedorov, *Phys. Met. Metall. USSR 29 (1970) 131-139.*

[34] P. Gumbsch, H. Gao, *Science 283 (1999) 965-968.*

[35] I.I. Papirov, E.S. Karpov, M.I. Palatnik, M.B. Mileskin, *Met. Sci. Heat. Treat. 26 (1984) 887-891*.
[36] M.R. Barnett, N. Stanford, A. Ghaderi, F. Siska, *Acta Mater. 61 (2013) 7859-7867*.

List of figure captions

Fig. 1 Microstructure (ED→) and texture (ED↑, TD→, levels: 1.0, 1.5, 2.0, 3.0, 5.0, 7.0 m.r.d.) of ZK10 magnesium alloy.

Fig. 2 True stress, strain hardening rate and the AE count rate vs. true strain curves for sample compressed along the ED (a), TD (b) and ND (c). The labels represent specific points for texture measurement.

Fig. 3 The evolution of crystallographic texture in ZK10 alloy (ED↑, TD→, levels: 1.0, 1.5, 2.0, 3.0, 5.0, 7.0, 9.0 m.r.d.): a) as extruded; and after compression along the ED up to: b) 60 MPa (after YS); c) 75 MPa; d) 100 MPa; e) 200 MPa; f) 250 MPa (position 0-5 in Fig. 2a).

Fig. 4 The evolution of crystallographic texture in ZK10 alloy (ED↑, TD→, levels: 1.0, 1.5, 2.0, 3.0, 5.0, 7.0 m.r.d.): a) as extruded; and after compression along the TD up to: b) 60 MPa (after YS); c) 85 MPa; d) 130 MPa; e) 190 MPa (position 0-4 in Fig. 2b).

Fig. 5 The evolution of crystallographic texture in ZK10 alloy (ED↑, TD→, levels: 1.0, 1.5, 2.0, 3.0, 5.0, 7.0 m.r.d.): a) as extruded; and after compression along the ND up to: b) 140 MPa; c) 220 MPa; (position 0-2 in Fig. 2c).

Fig. 6: Example for different types of signals; a) continuous signal, b) burst signal.

Fig. 7 Dependence of energy on the median frequency for sample compressed along: a) ED, b) TD, c) ND.

Fig. 8 The number of elements vs. time in the AE clusters for sample compressed along a) ED, b) TD and c) ND.

Fig. 9 The cumulative energy vs. time in the AE clusters for sample compressed along a) ED, b) TD and c) ND.

Table 1 Mechanical properties of extruded ZK10 magnesium alloy deformed along various axes; CYS – compressive yield strength, UCS – ultimate compressive stress.

Table 2 Remarks for the texture measurements.

Highlights

- Acoustic emission analysis allows revealing preferred deformation mechanisms.
- Twinning dominates deformation during extrusion and transversal compression.
- Non-basal slip becomes the main deformation mechanism for higher strains.
- Basal and non-basal slips proceed simultaneously during normal compression.

Tables

Mg alloy	Sample orientation	CYS (MPa)	UCS (MPa)	Uniform elongation (%)	Fracture strain (%)
ZK10	ED	54 (±2)	293 (±2)	8.5 (±0.3)	8.8 (±0.3)
	TD	52 (±3)	252 (±2)	4.6 (±0.3)	5.1 (±0.3)
	ND	120 (±5)	259 (±2)	5.8 (±0.3)	9.0 (±0.3)

Table 1 Mechanical properties of extruded ZK10 magnesium alloy deformed along various axes; CYS – compressive yield strength, UCS – ultimate compressive stress.

	ED		**TD**		**ND**	
	Stress	Remark	Stress	Remark	Stress	Remark
Position 1	70	after the yield point	75	after the yield point	140	after the yield point
Position 2	75	minimum of hardening rate	85	minimum of hardening rate	220	ongoing deformation
Position 3	100	after the disappearance AE signal	130	after the disappearance AE signal		
Position 4	200	maximum of hardening rate (inflection point)	190	maximum of hardening rate (inflection point)		
Position 5	250	after the inflection point				

Table 2 Remarks for the texture measurements

Figure 1 color

Click here to download high resolution image

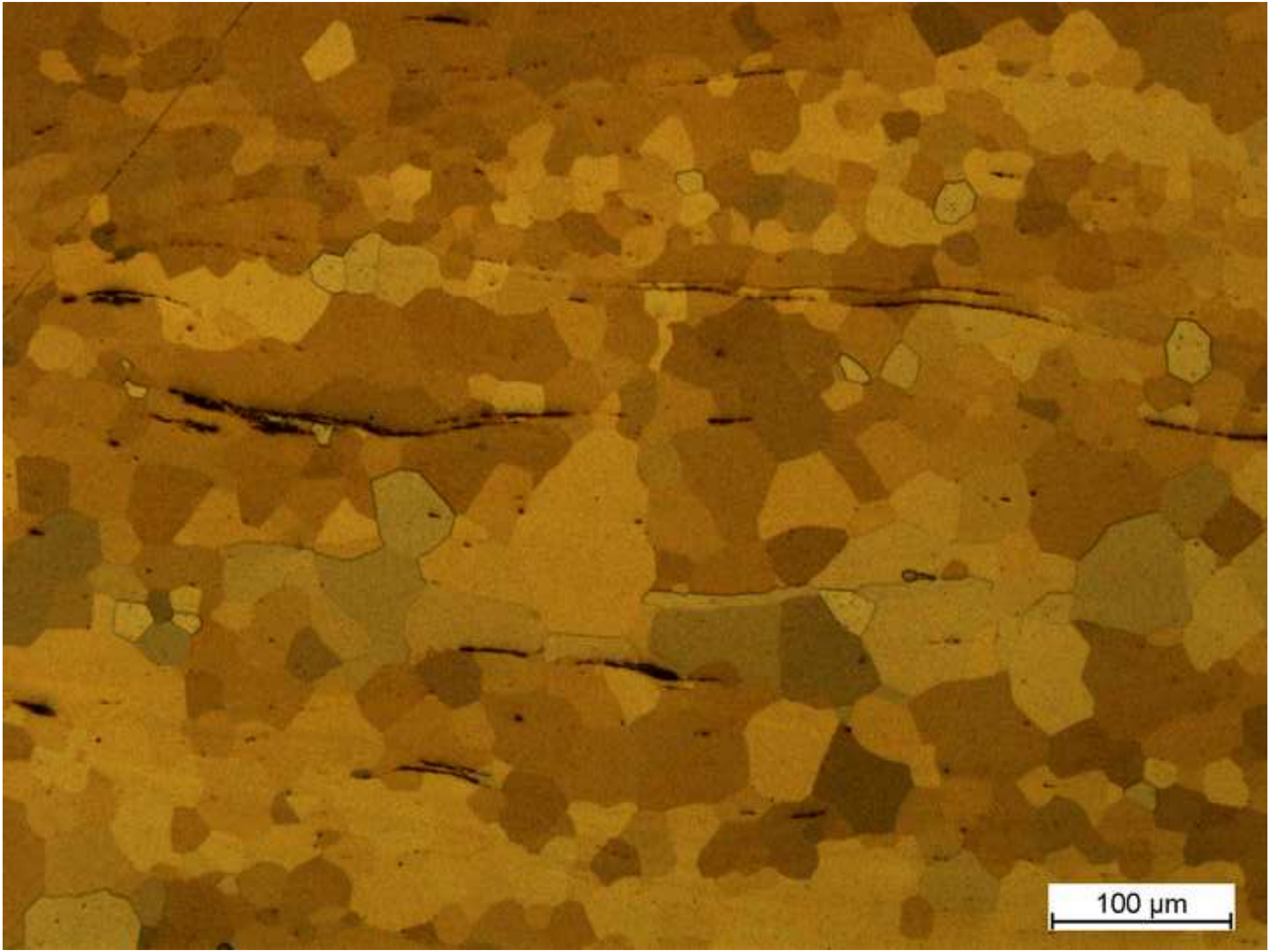

Figure 1

Click here to download high resolution image

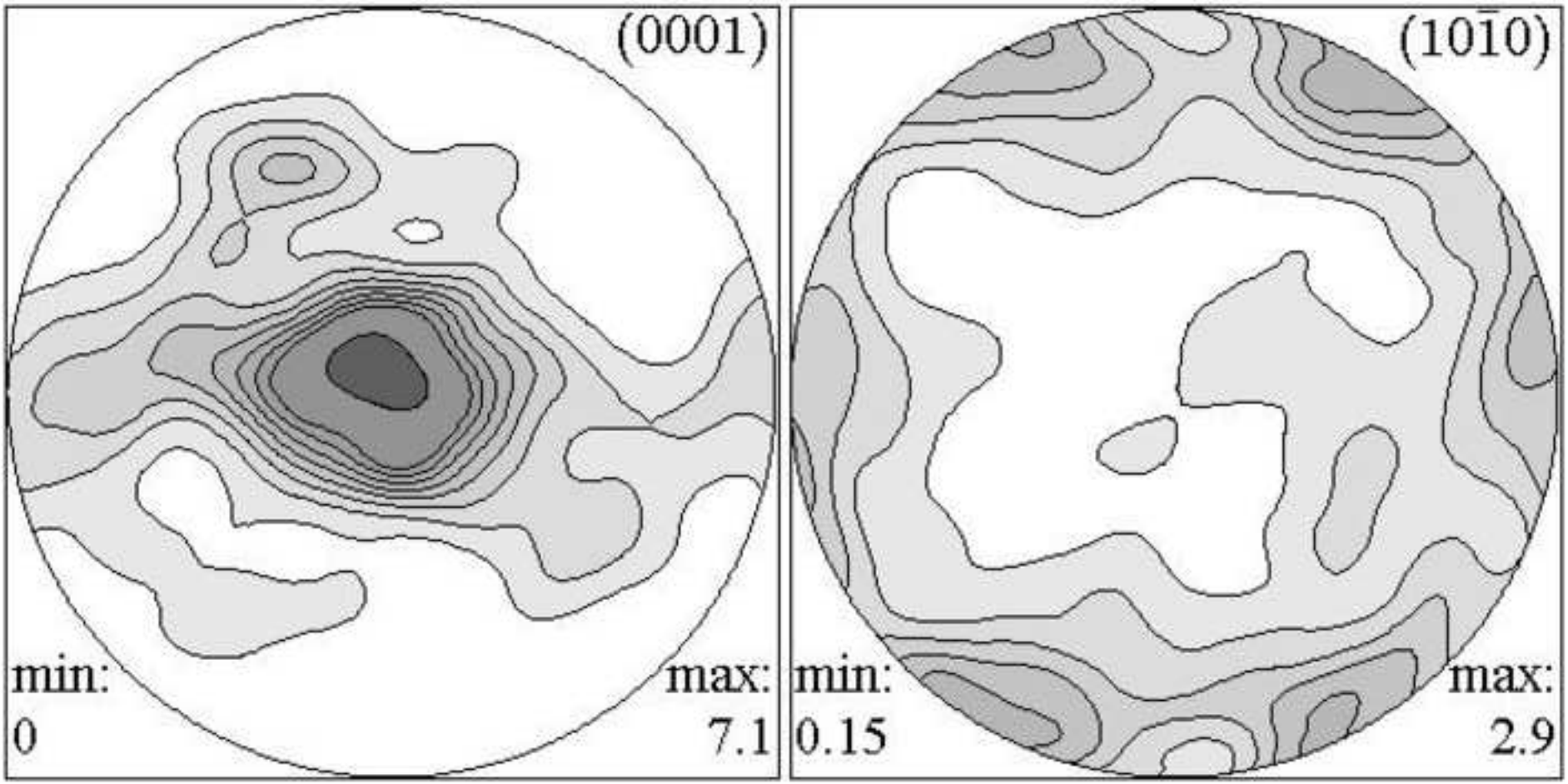

Figure 2a

Click here to download high resolution image

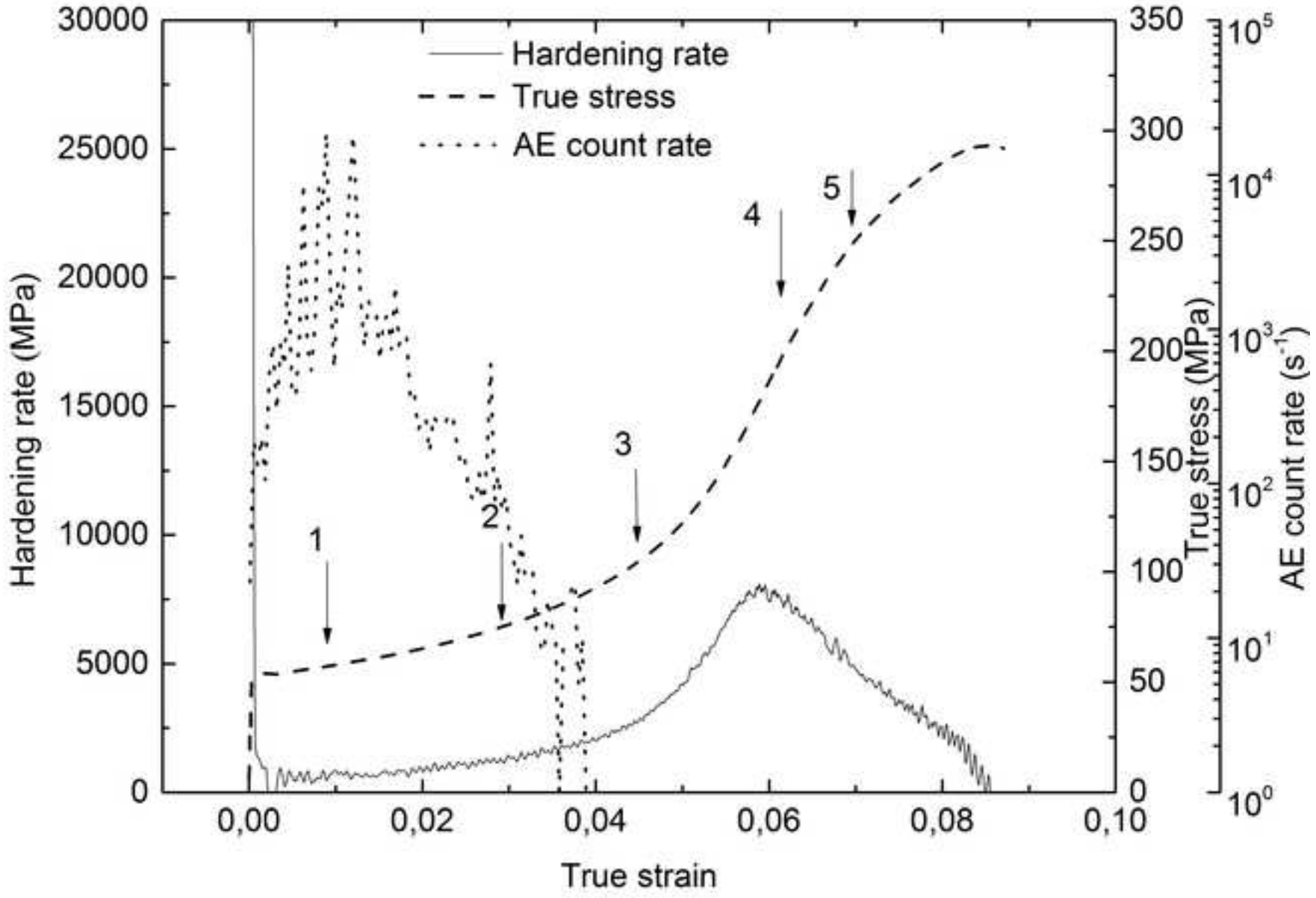

Figure 2b

Click here to download high resolution image

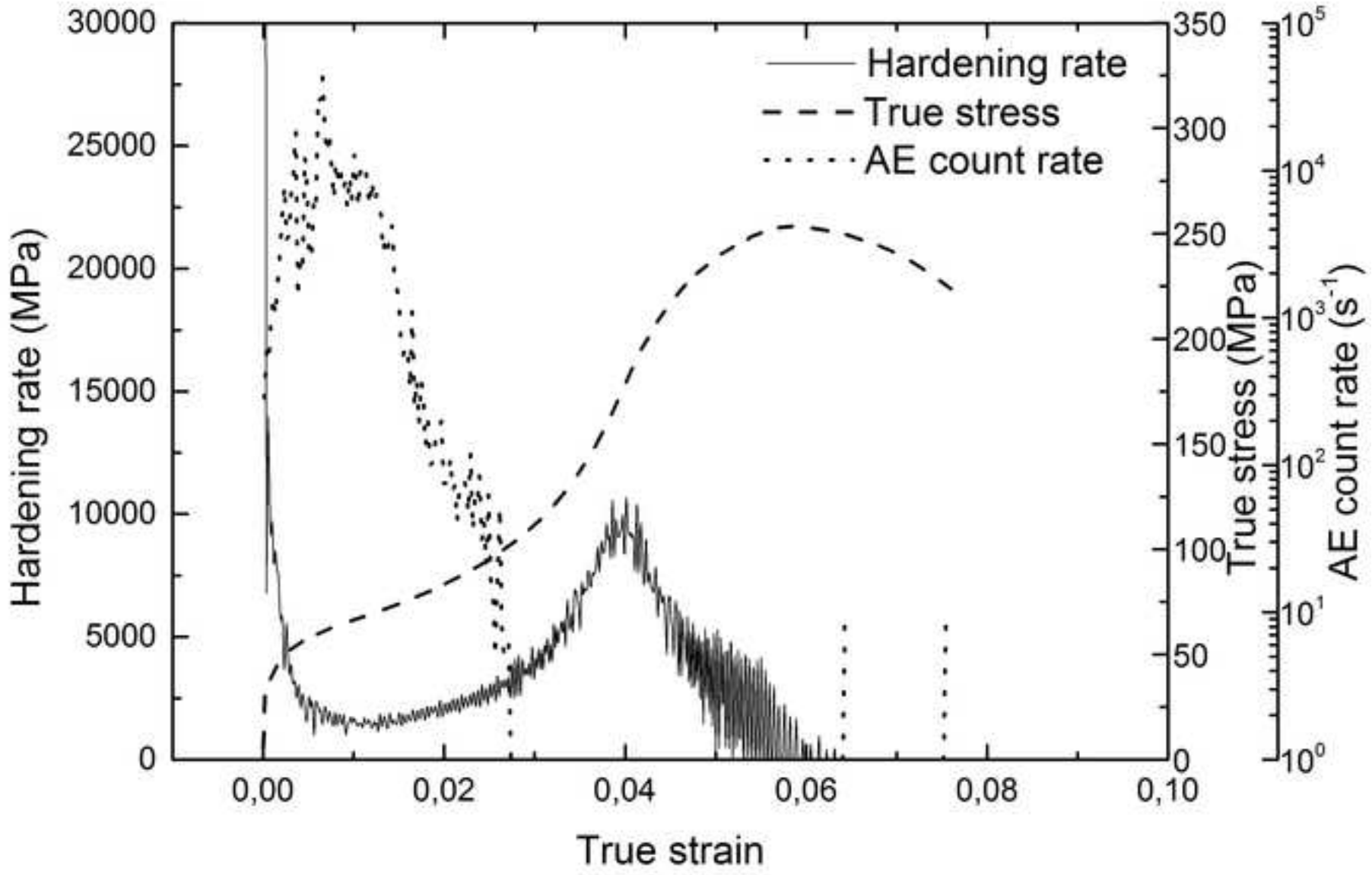

Figure 2c
Click here to download high resolution image

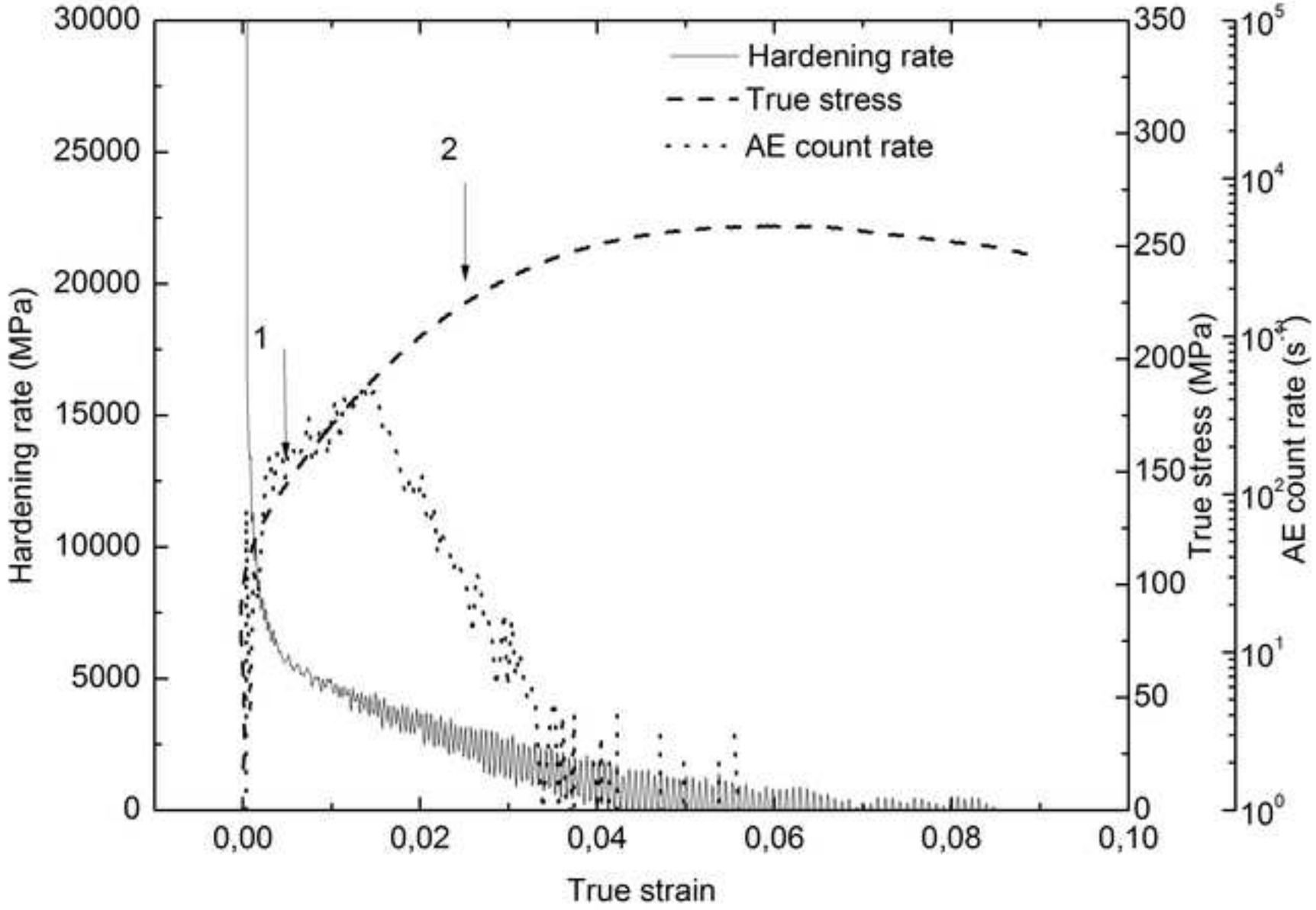

Figure 3a

Click here to download high resolution image

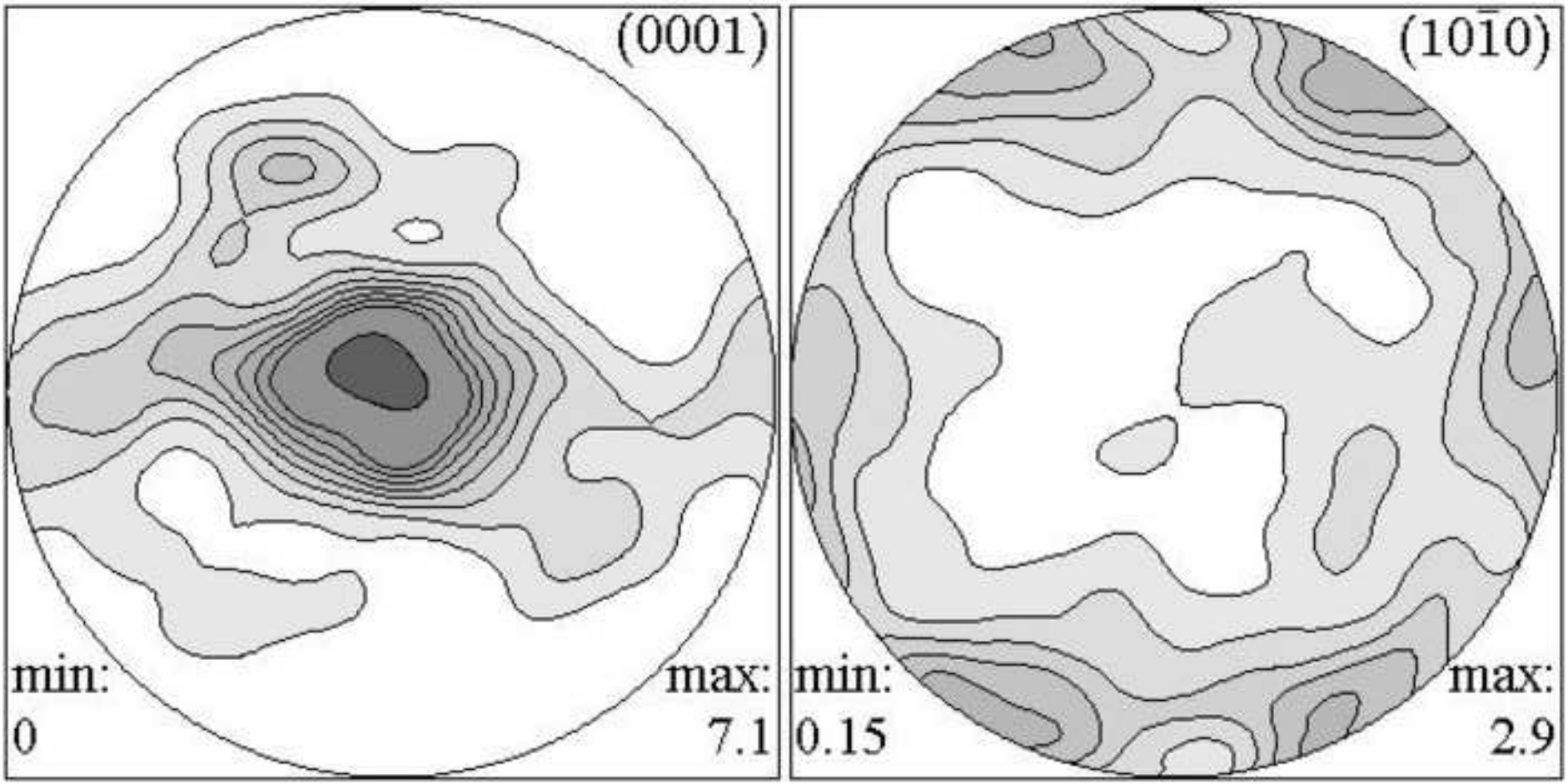

Figure 3b

Click here to download high resolution image

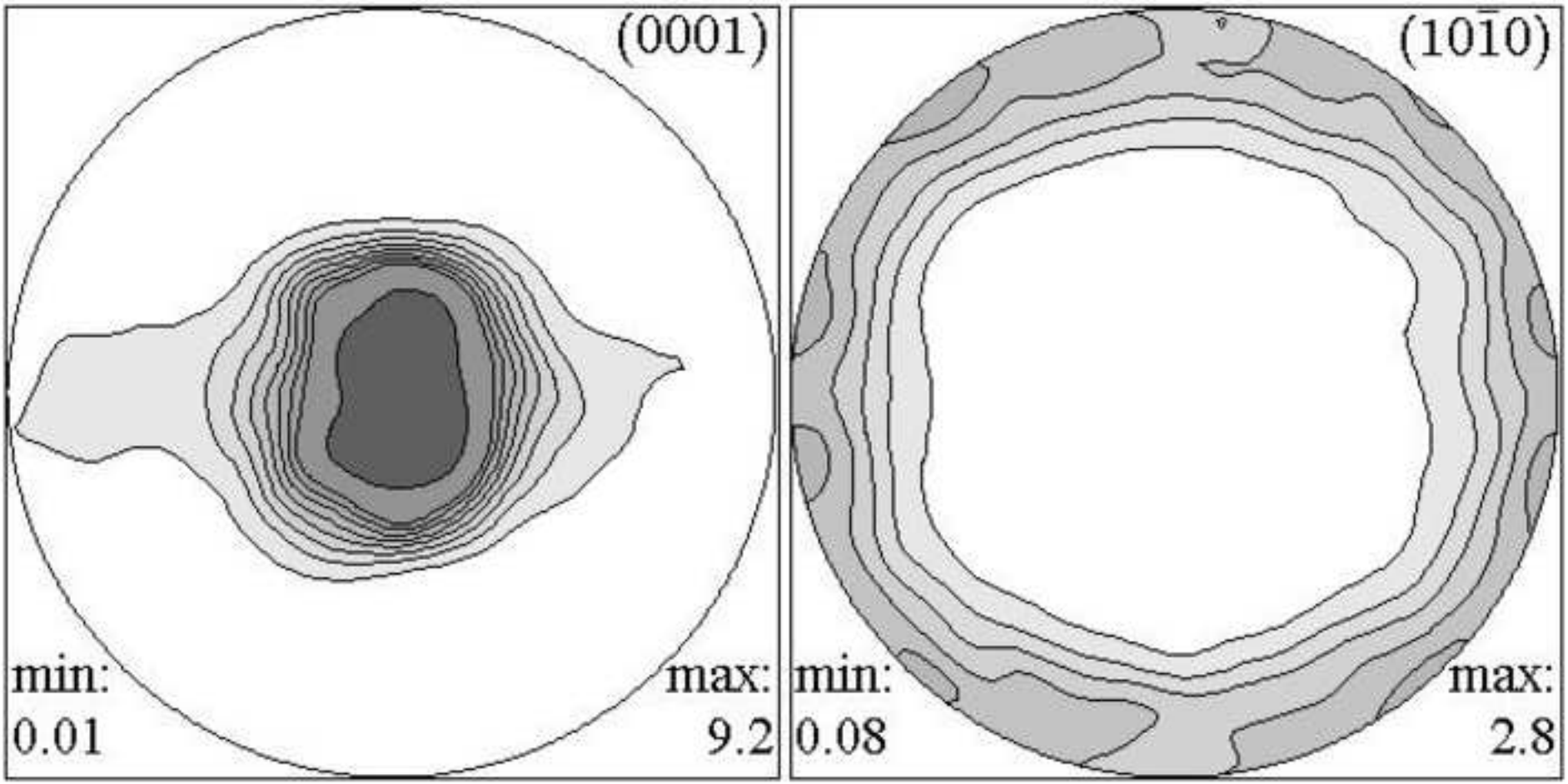

Figure 3c

Click here to download high resolution image

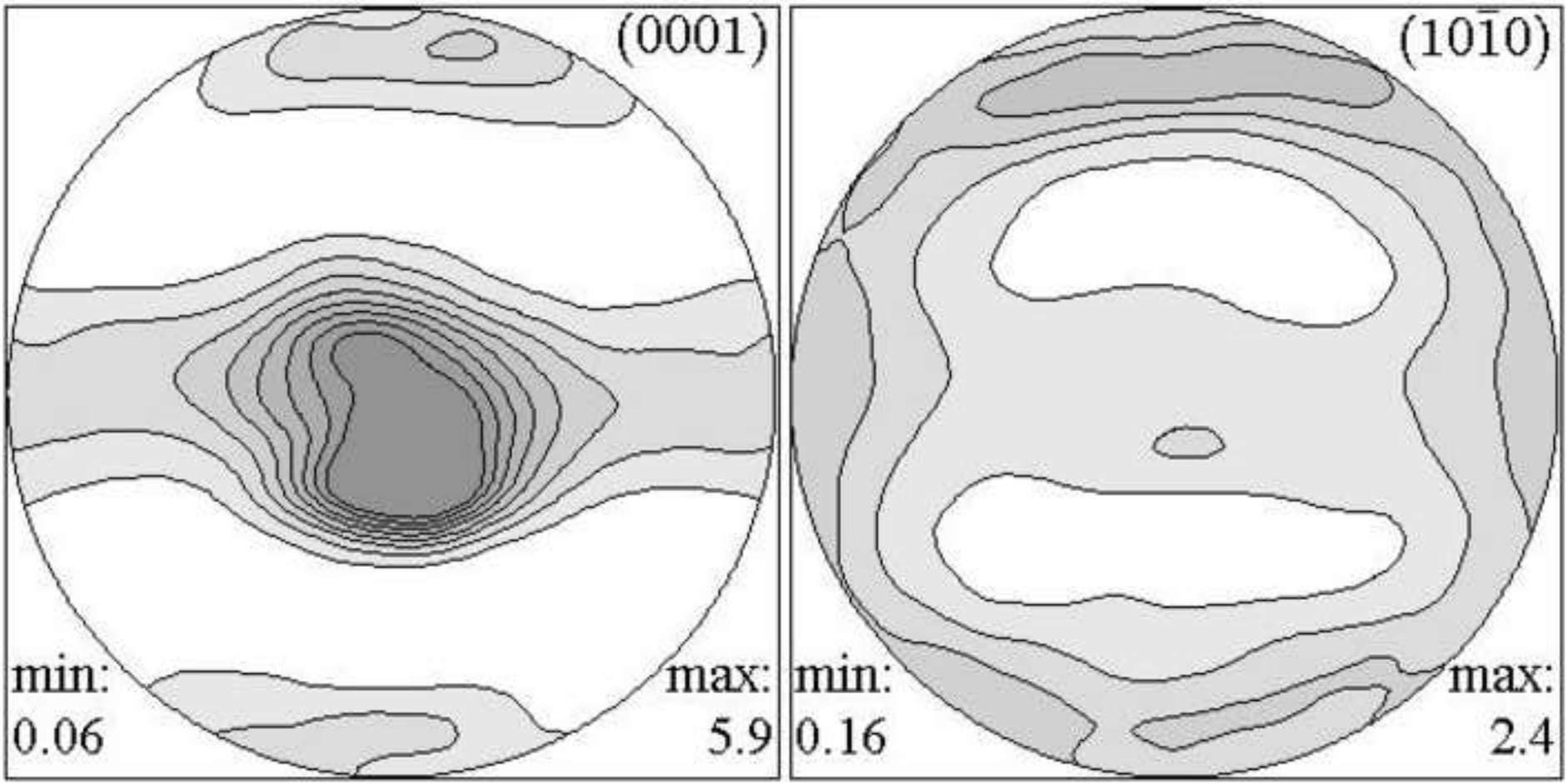

Figure 3d

Click here to download high resolution image

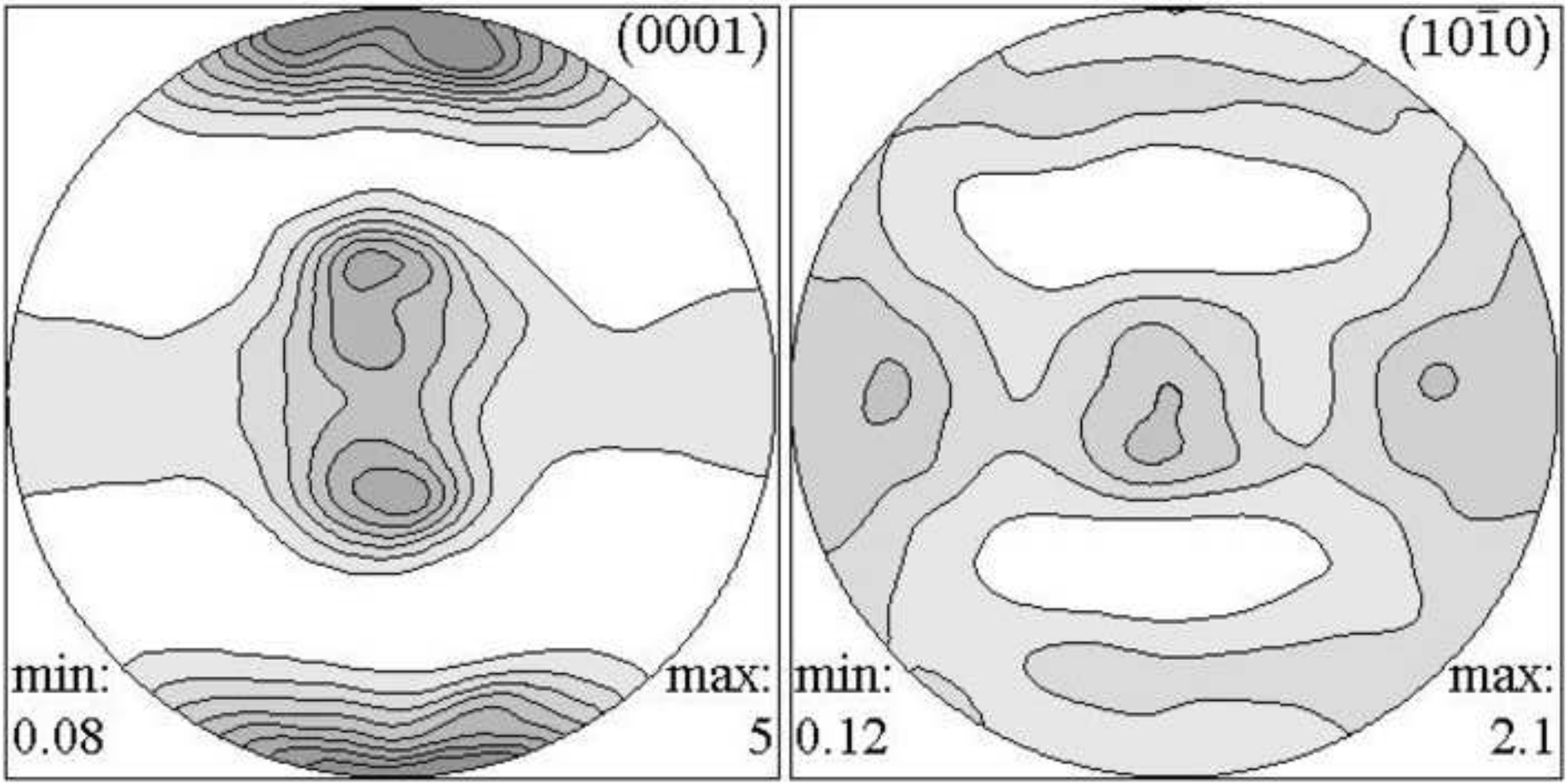

Figure 3e

Click here to download high resolution image

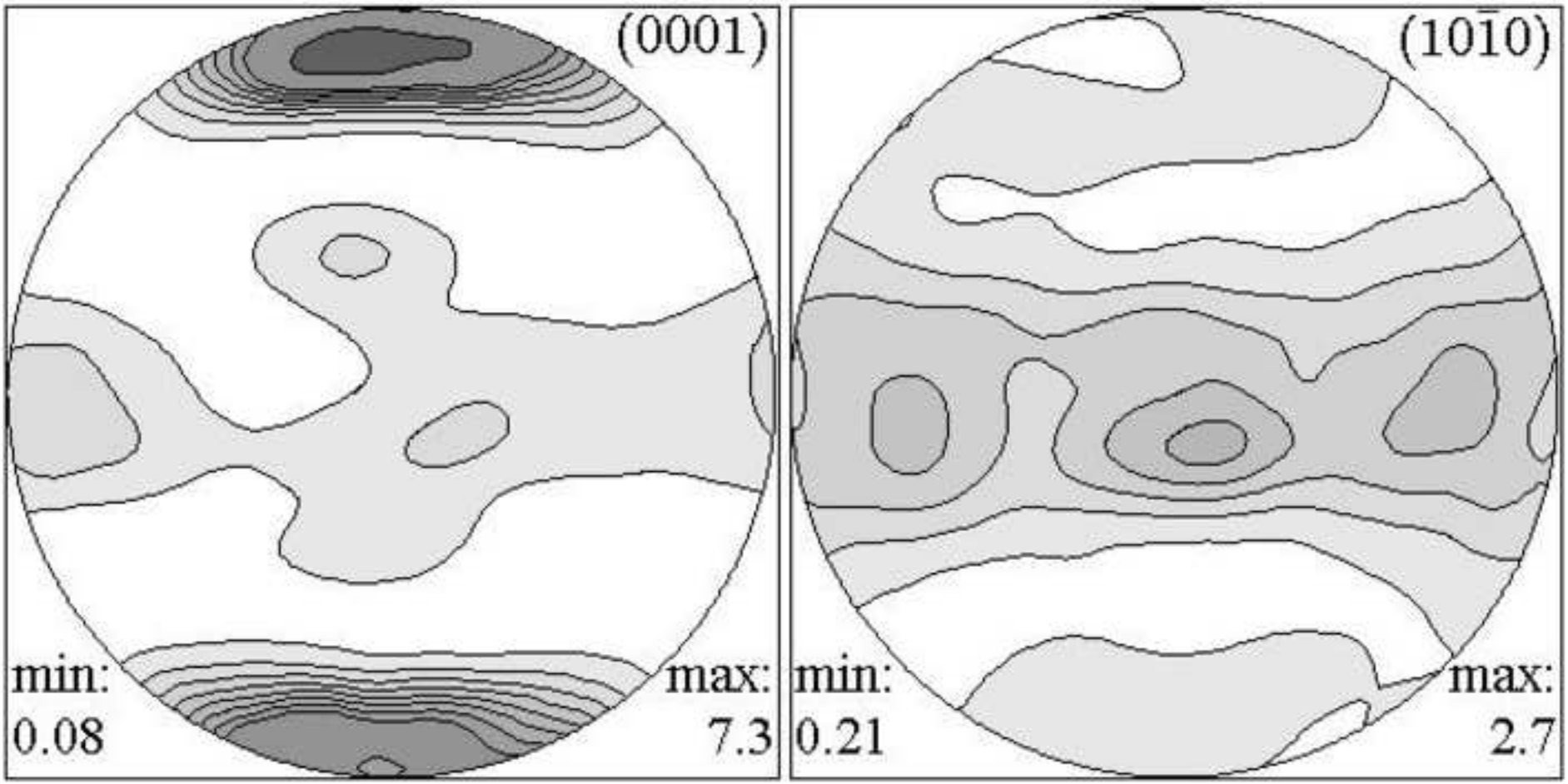

Figure 3f

Click here to download high resolution image

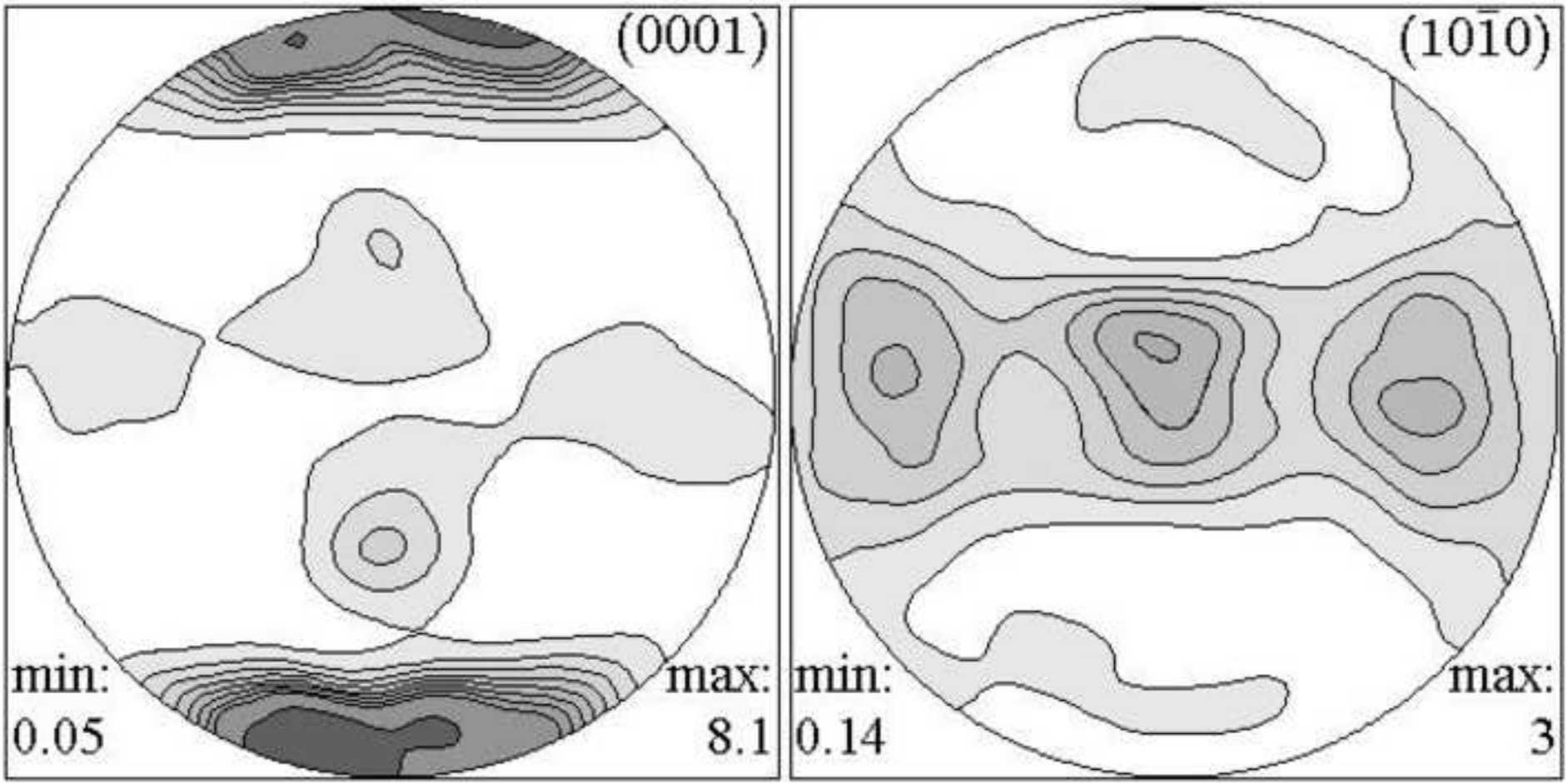

Figure 4a

Click here to download high resolution image

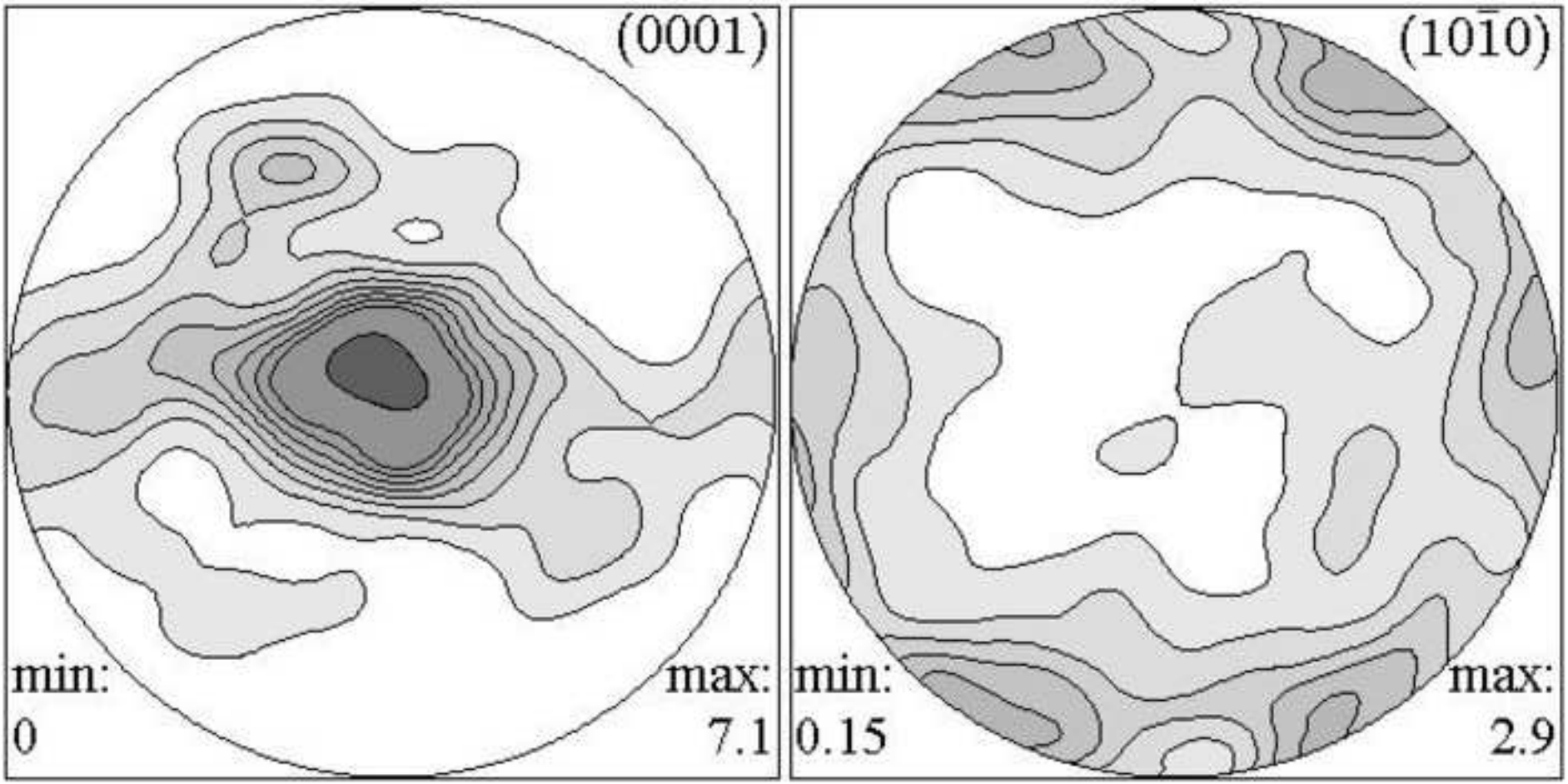

Figure 4b

Click here to download high resolution image

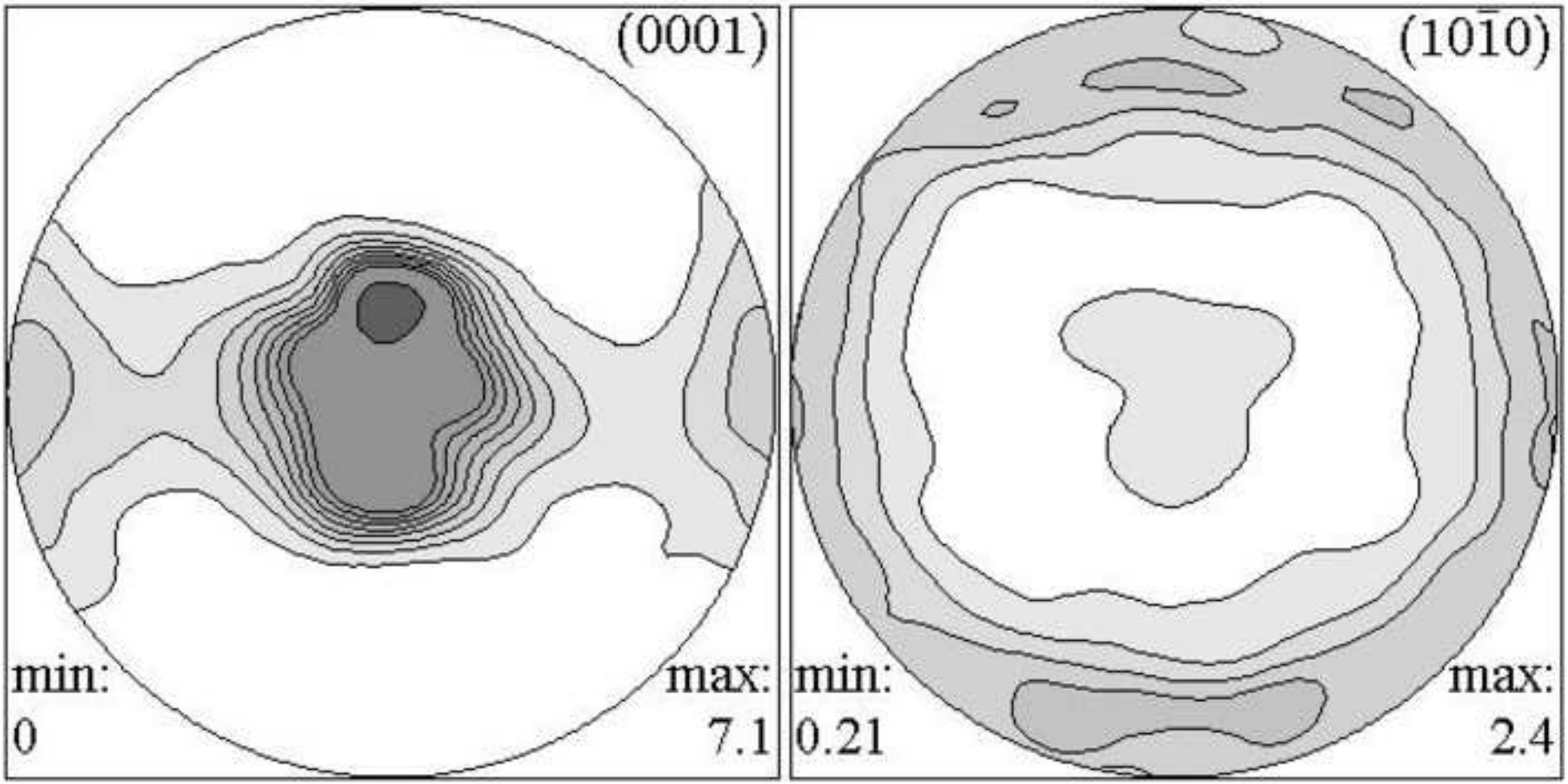

Figure 4c

Click here to download high resolution image

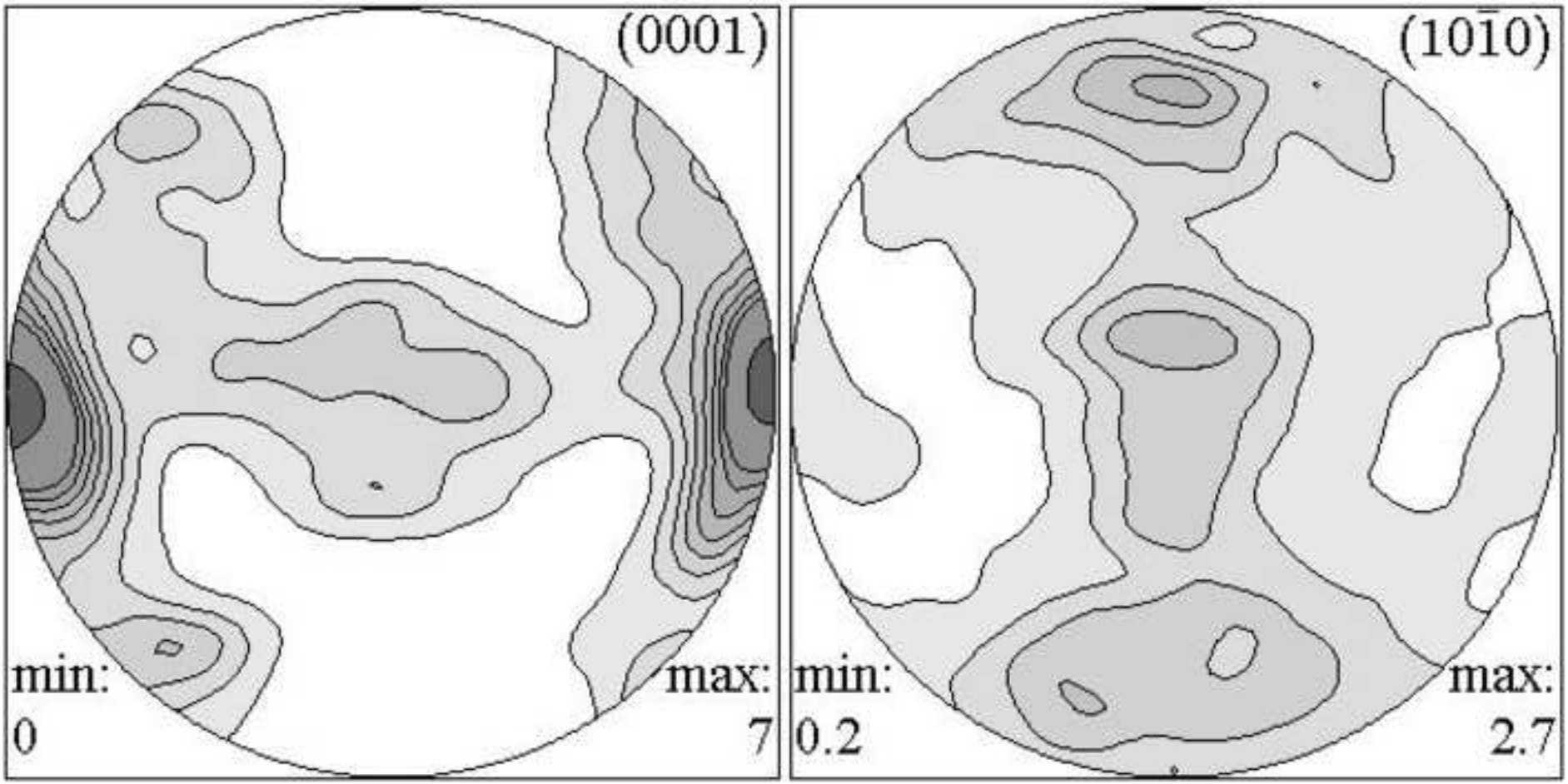

Figure 4d

Click here to download high resolution image

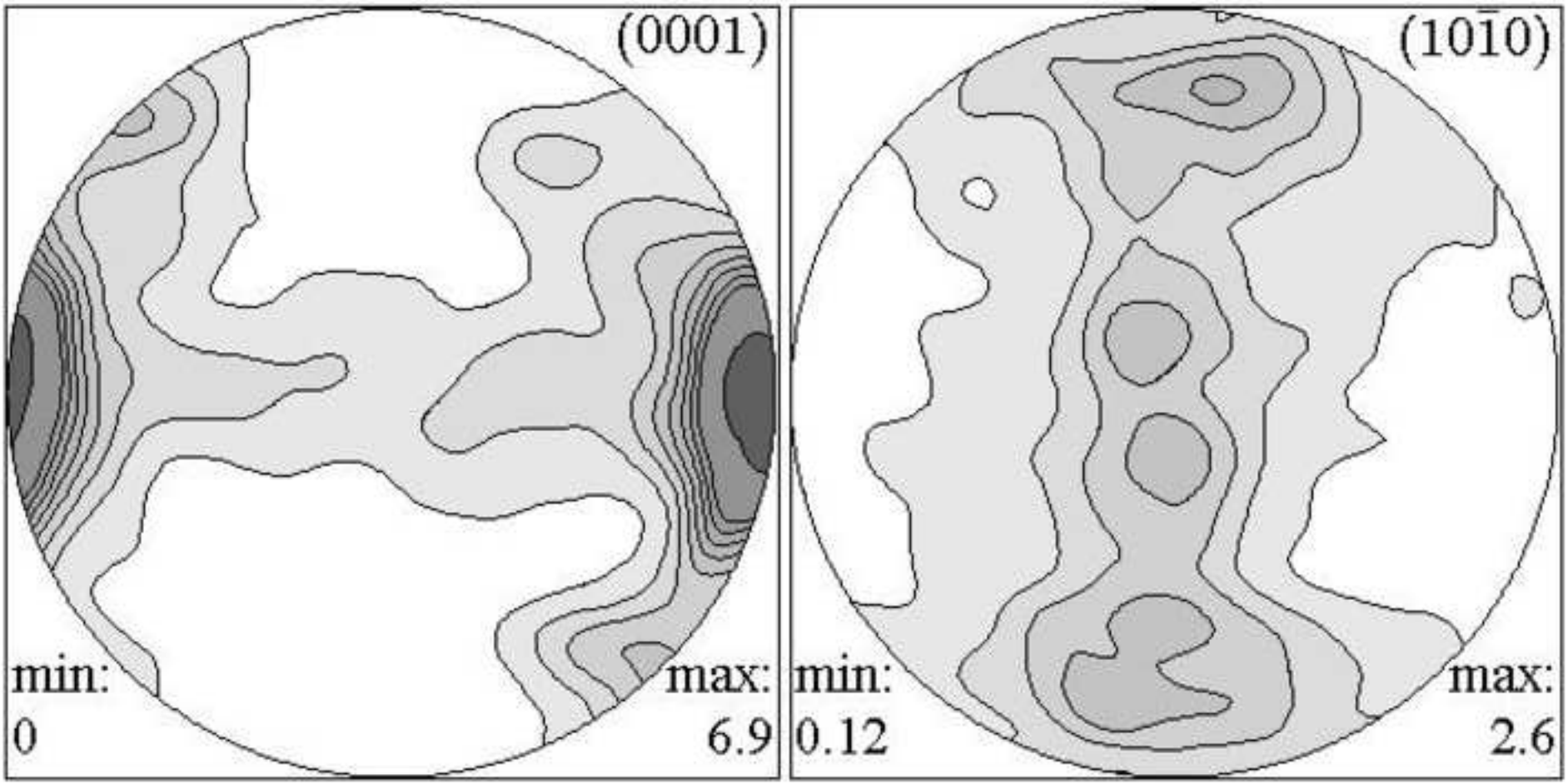

Figure 4e

Click here to download high resolution image

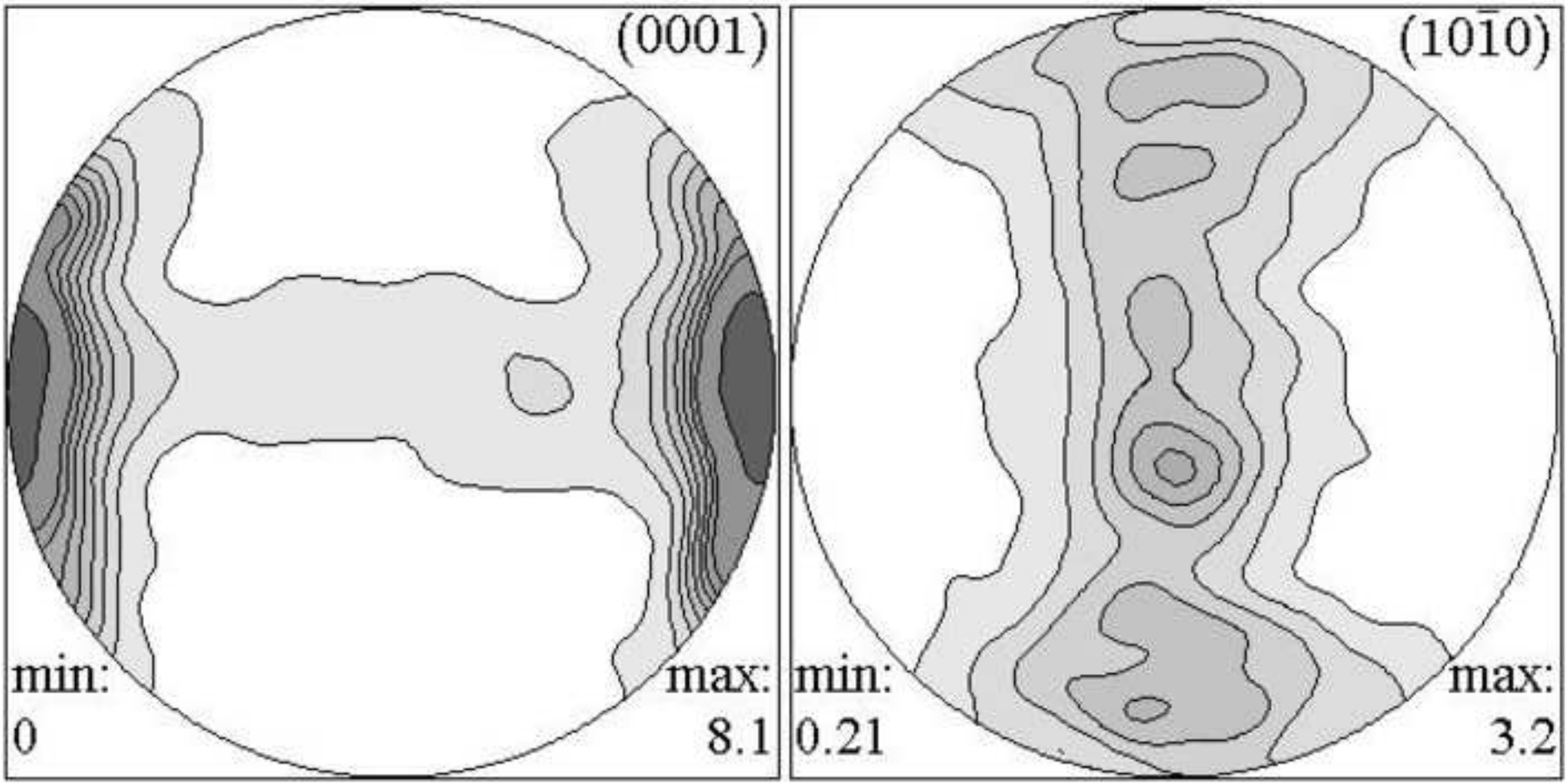

Figure 5a

Click here to download high resolution image

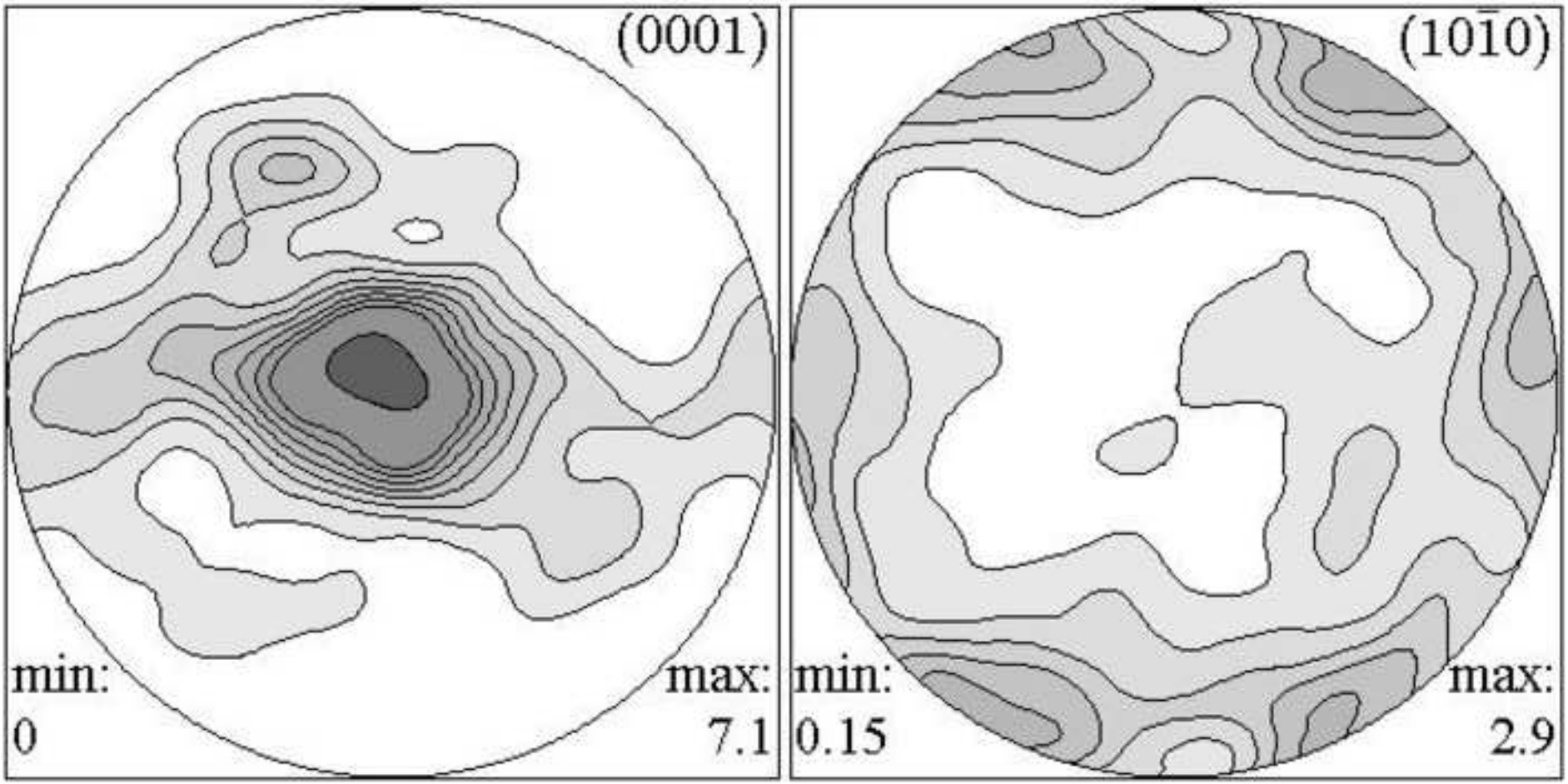

Figure 5b

Click here to download high resolution image

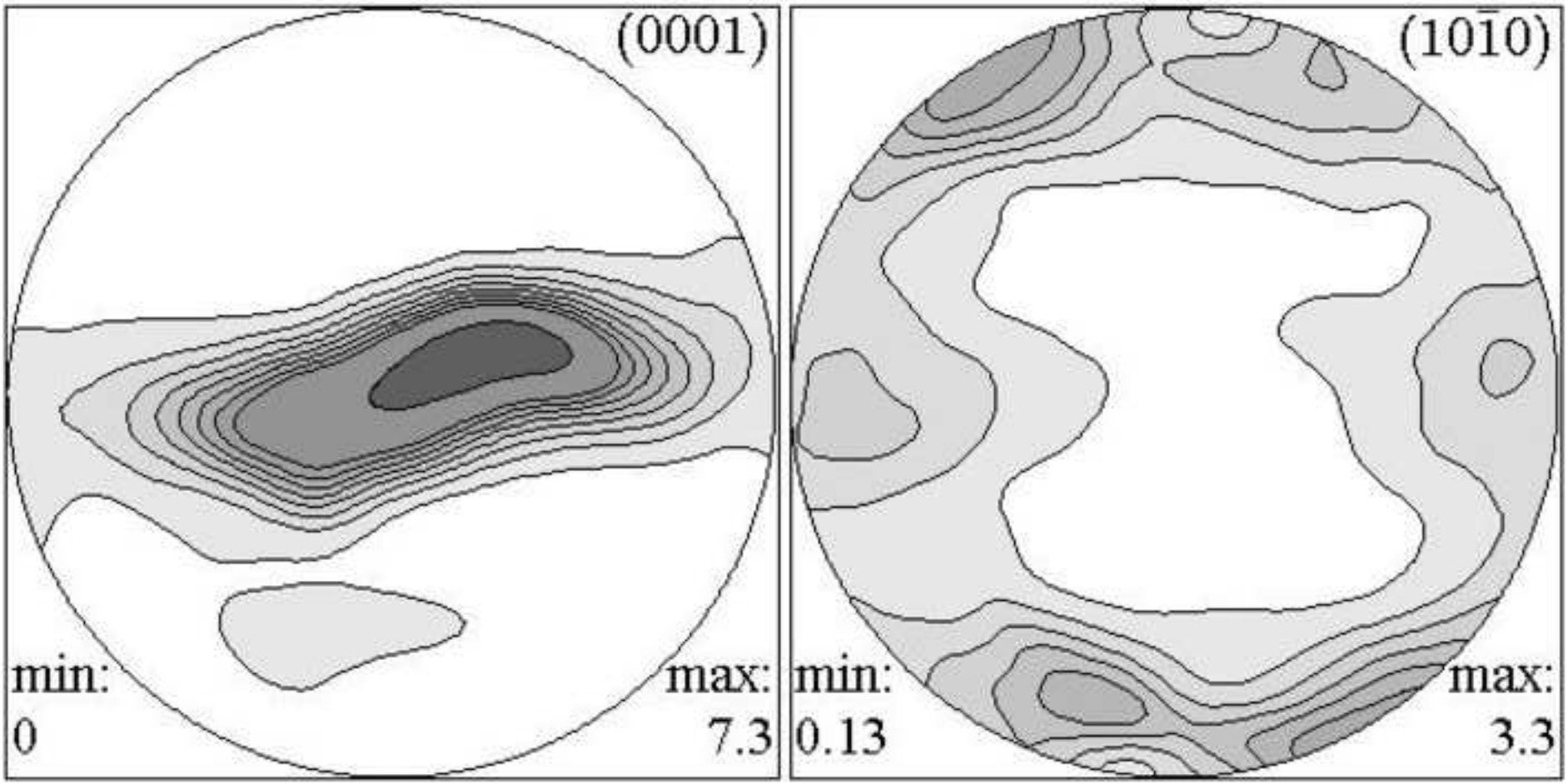

Figure 5c

Click here to download high resolution image

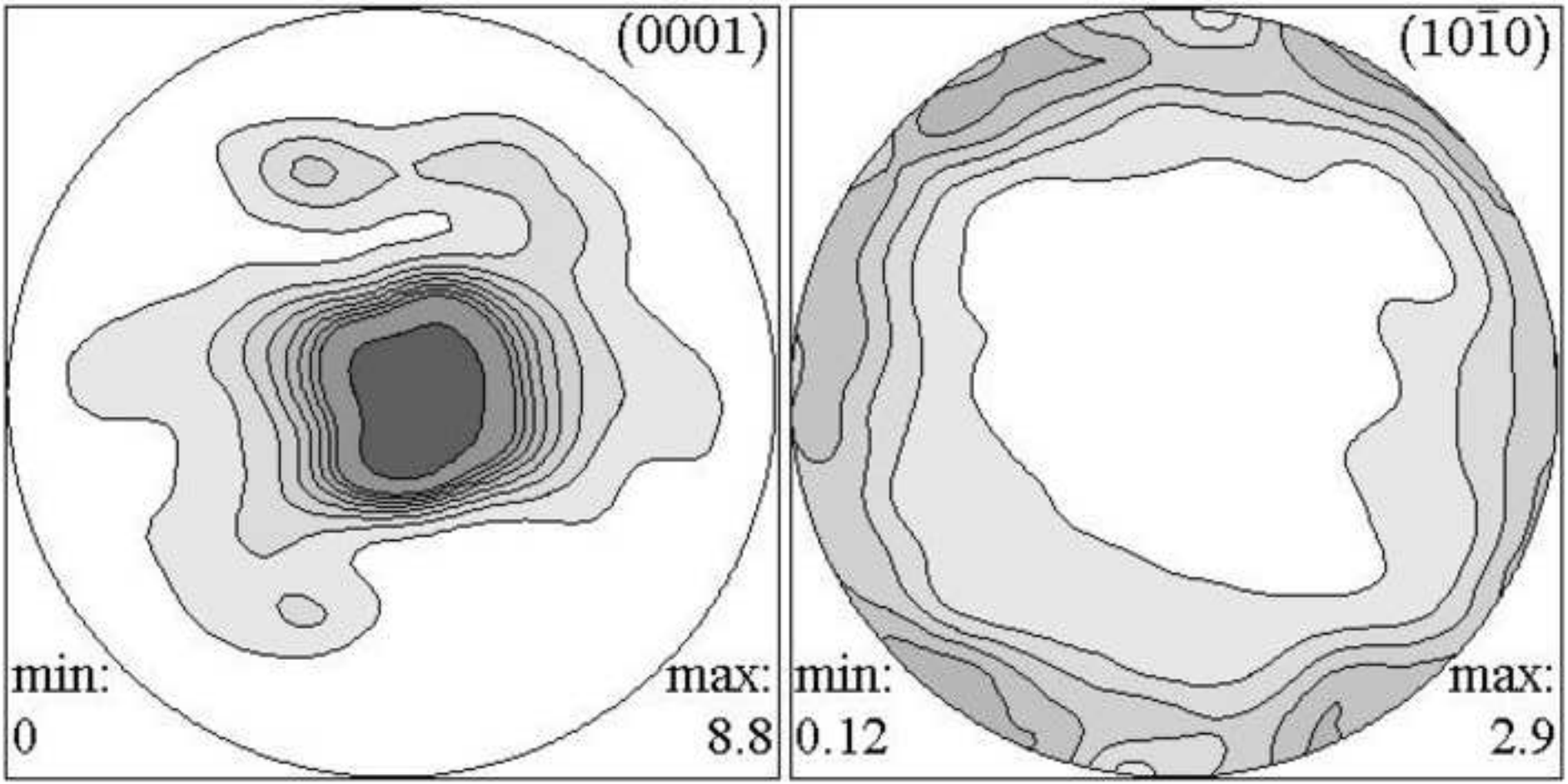

Figure 6a

Click here to download high resolution image

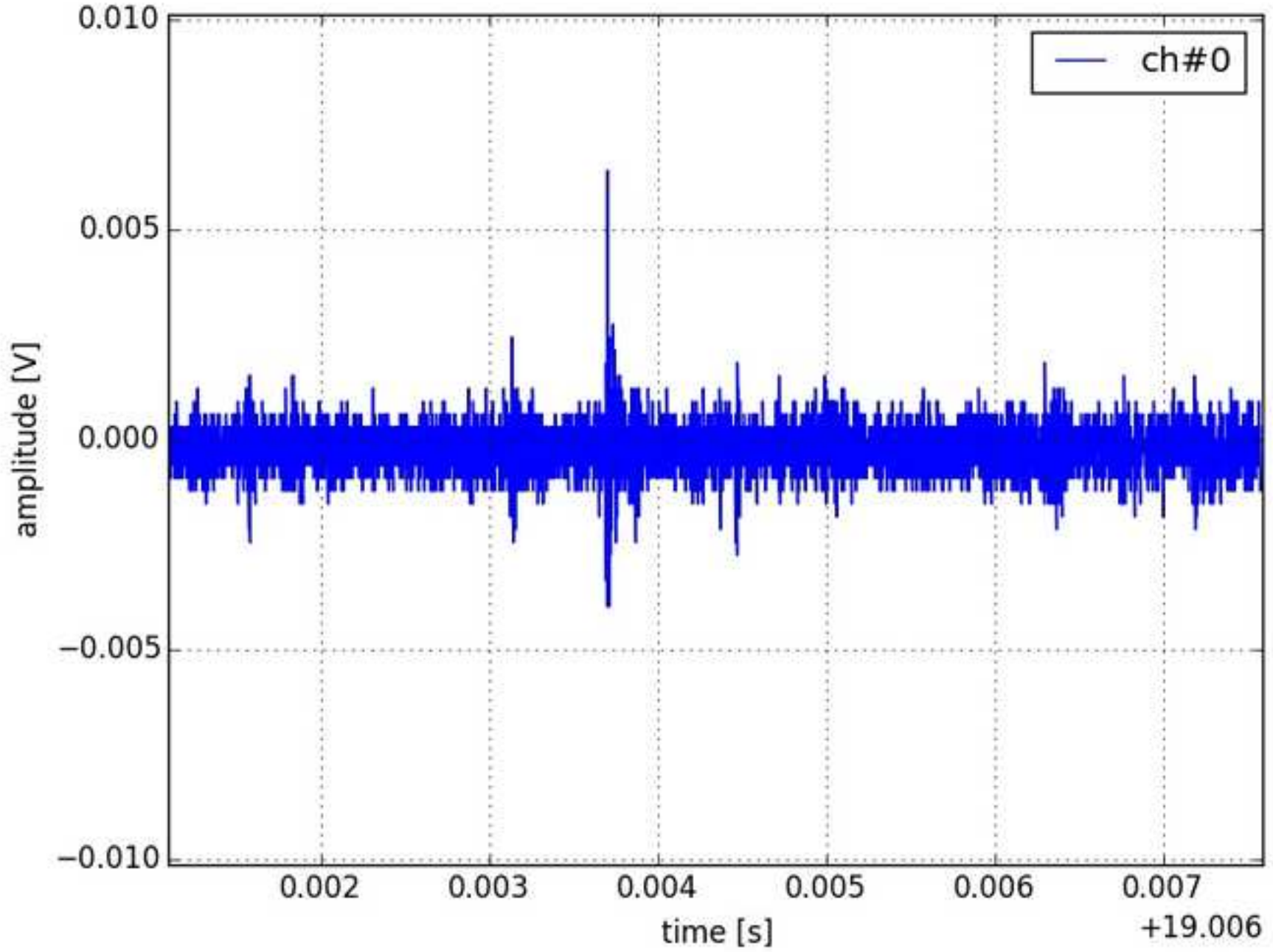

Figure 6b

Click here to download high resolution image

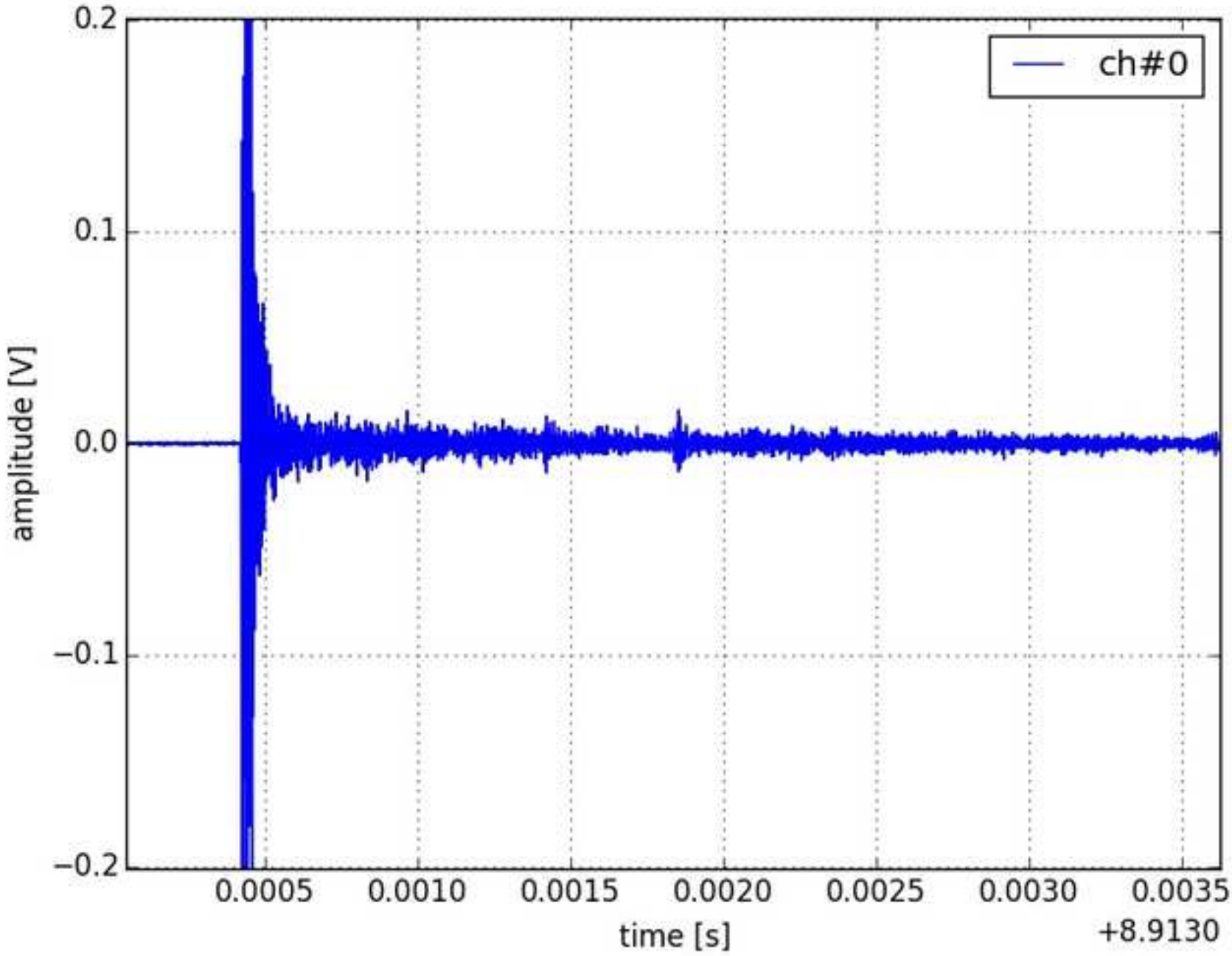

Figure 7a
Click here to download high resolution image

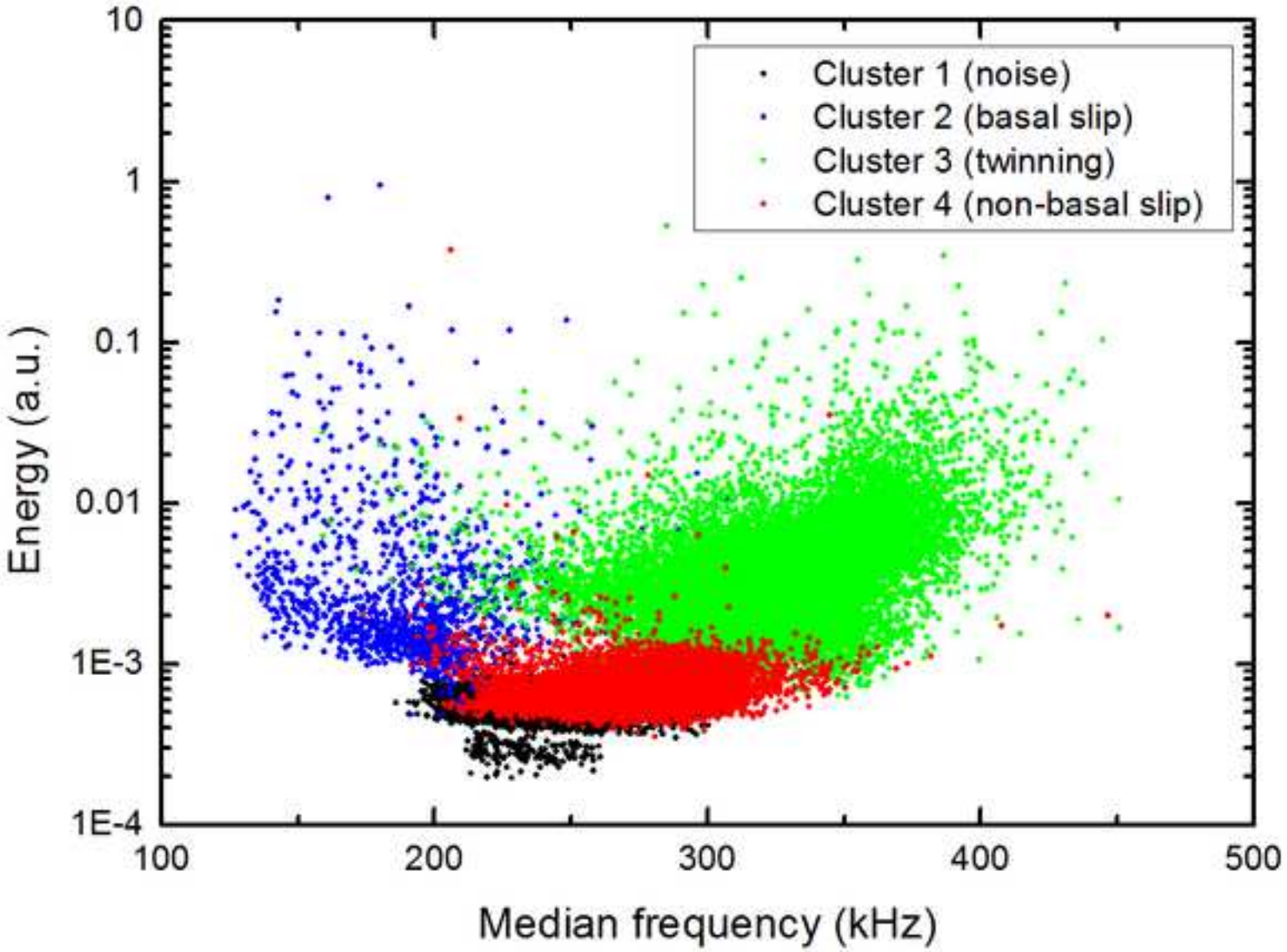

Figure 7b
Click here to download high resolution image

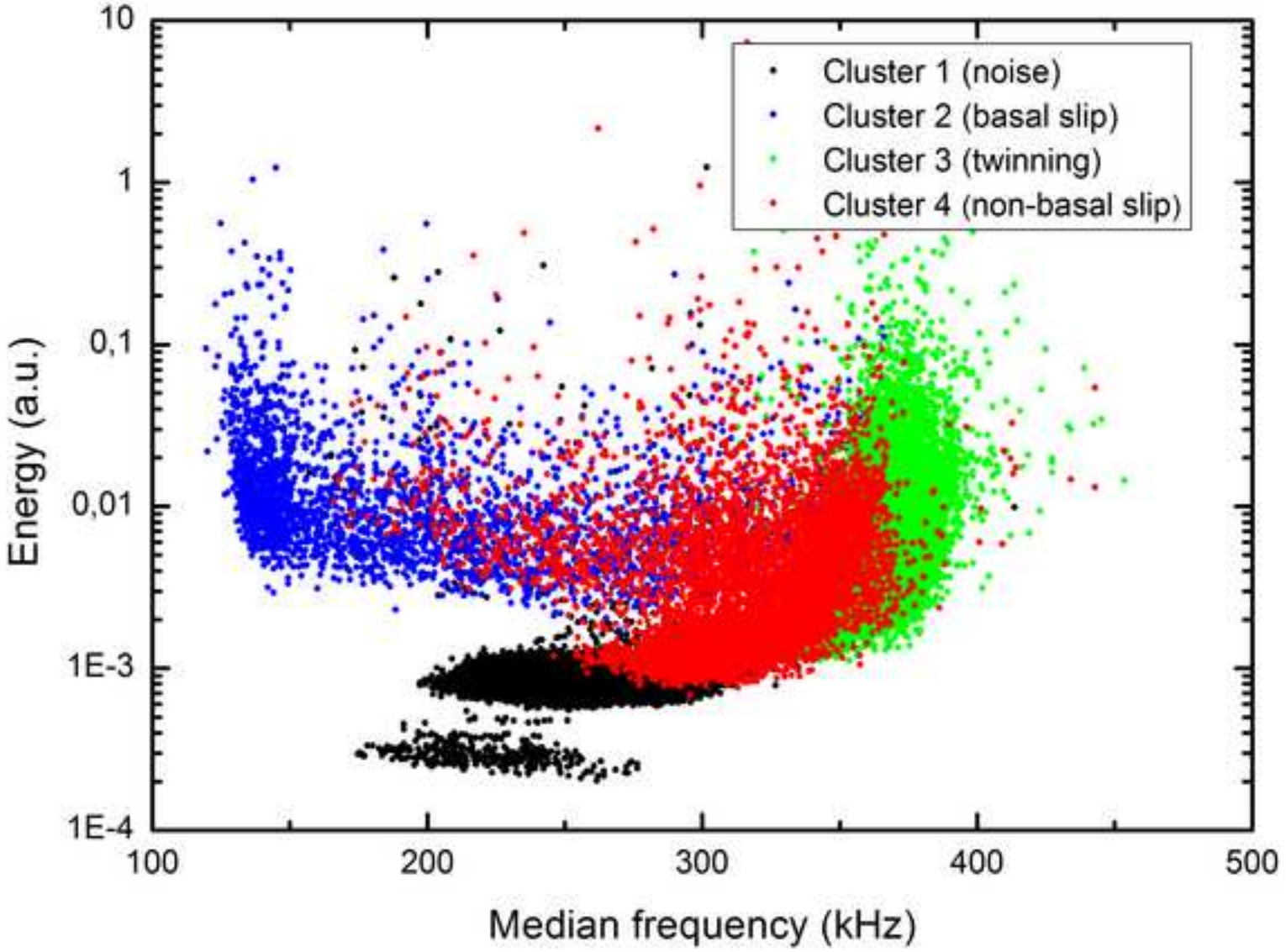

Figure 7c

Click here to download high resolution image

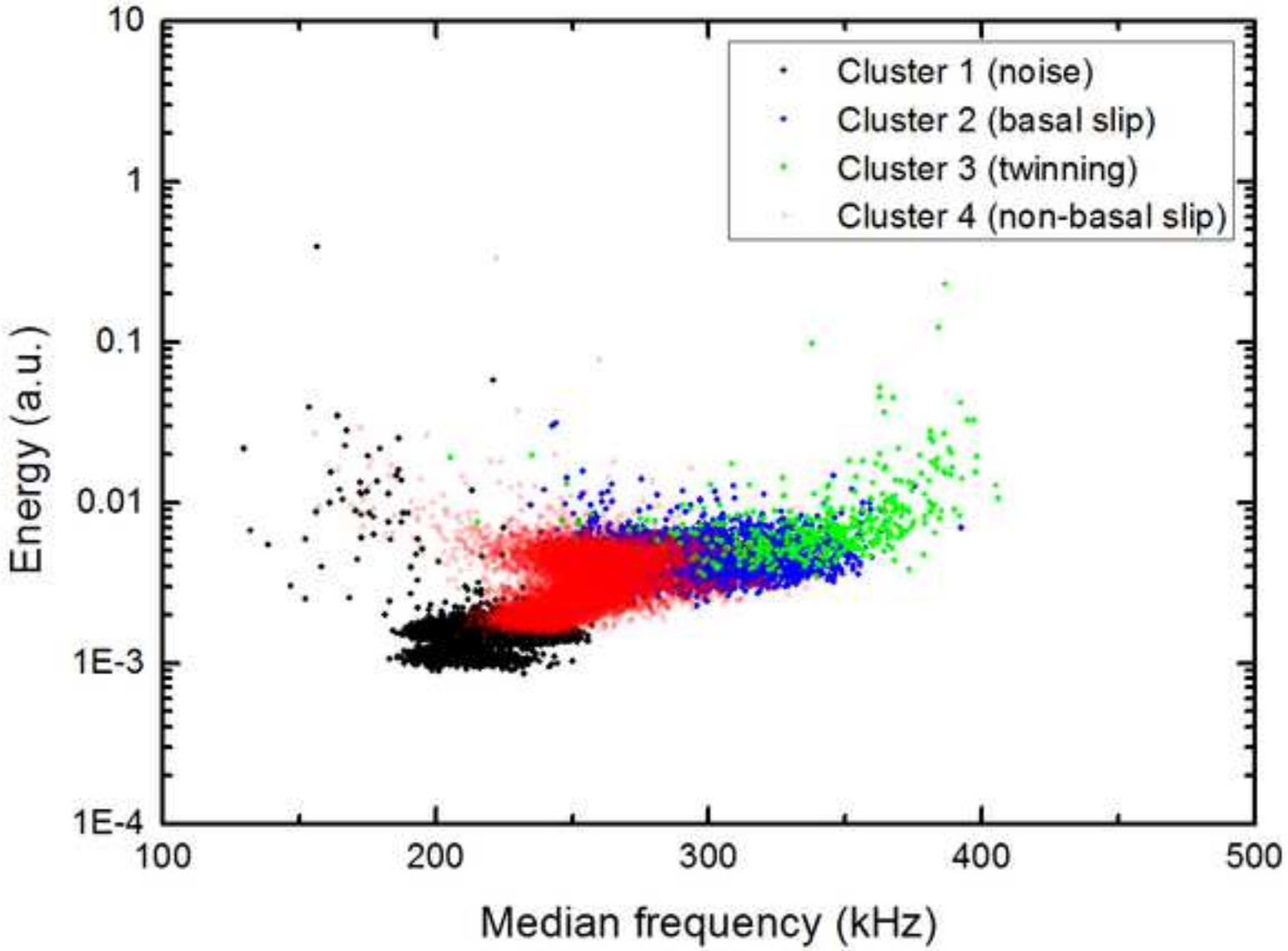

Figure 8a
Click here to download high resolution image

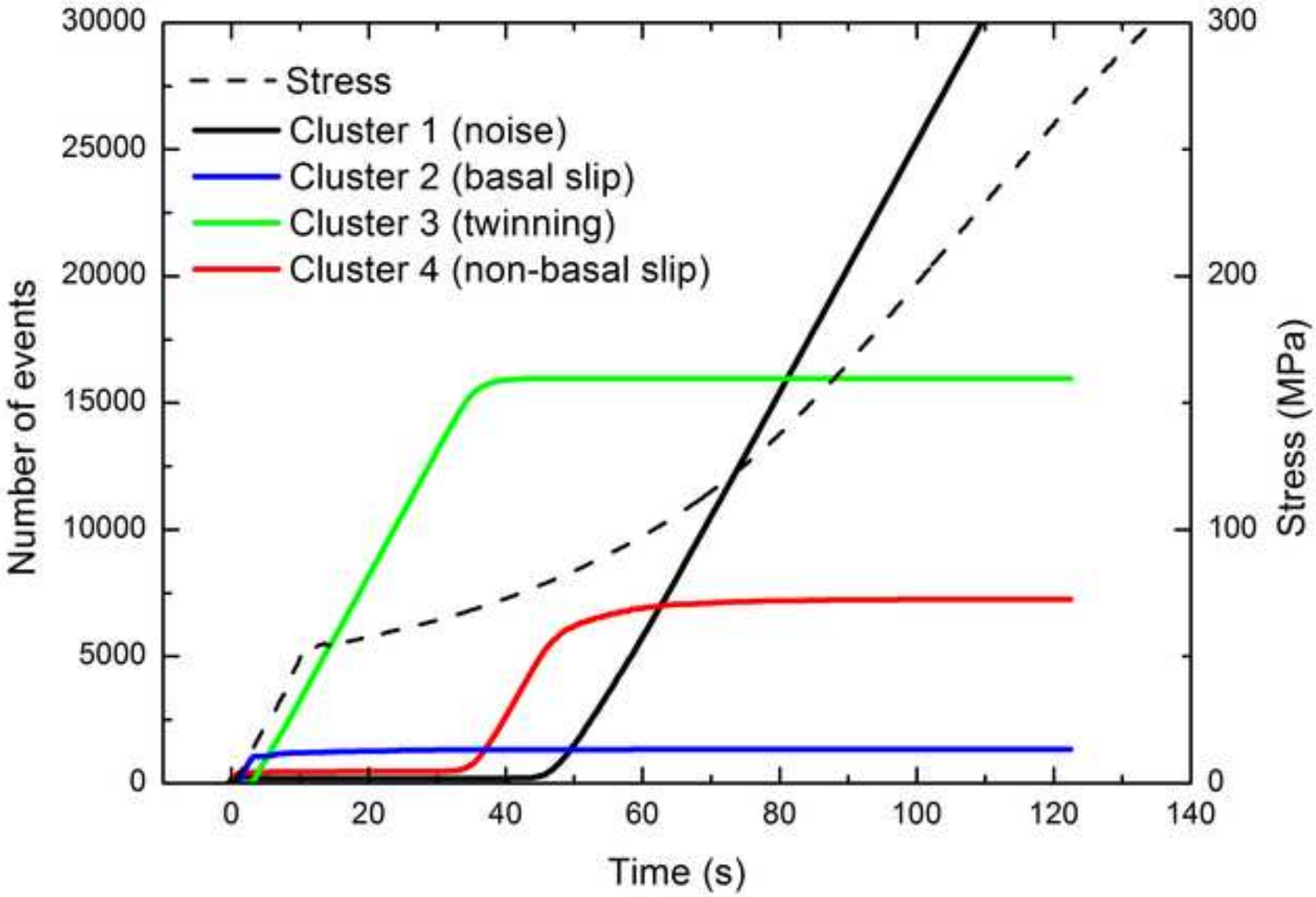

Figure 8b

Click here to download high resolution image

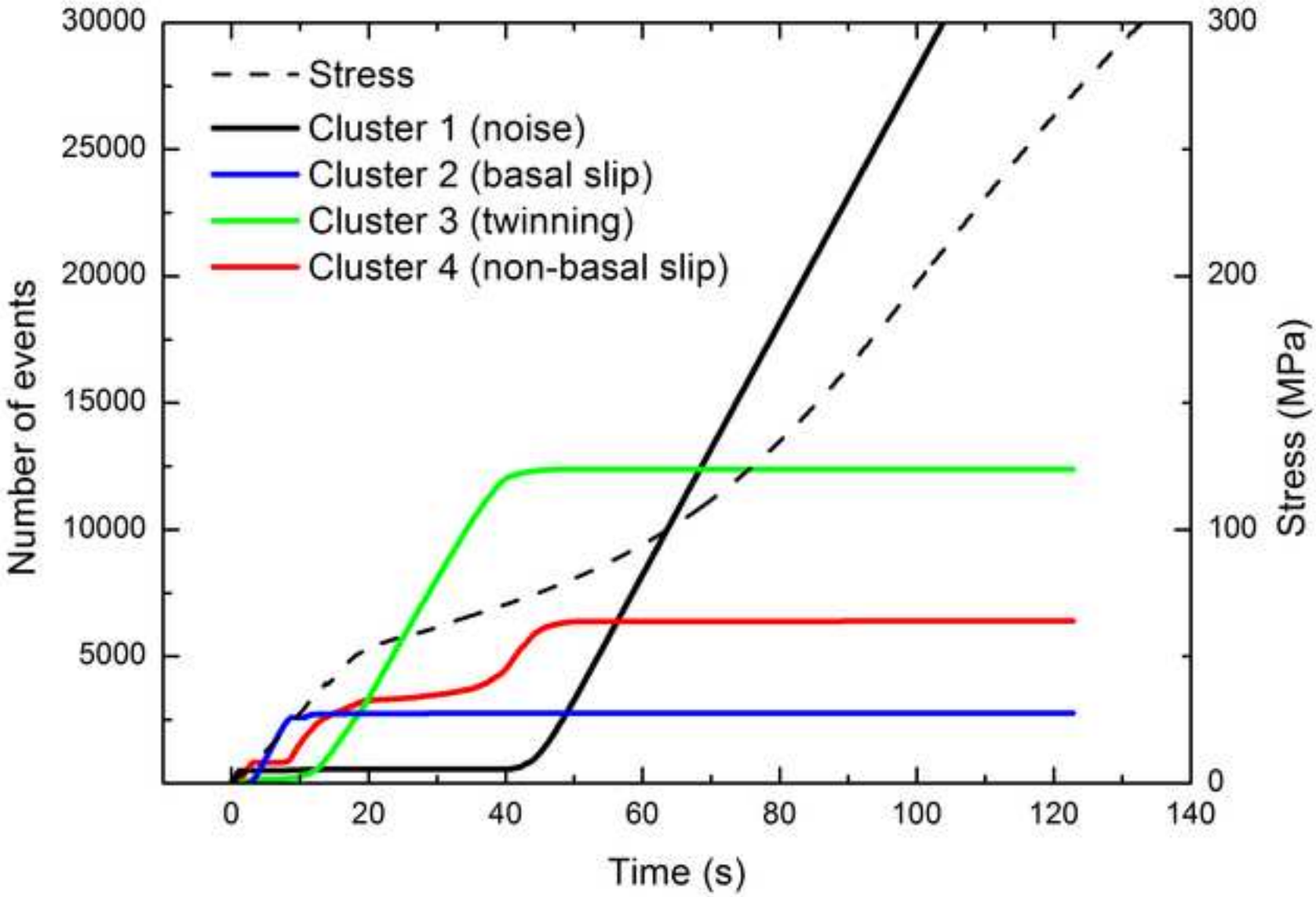

Figure 8c
Click here to download high resolution image

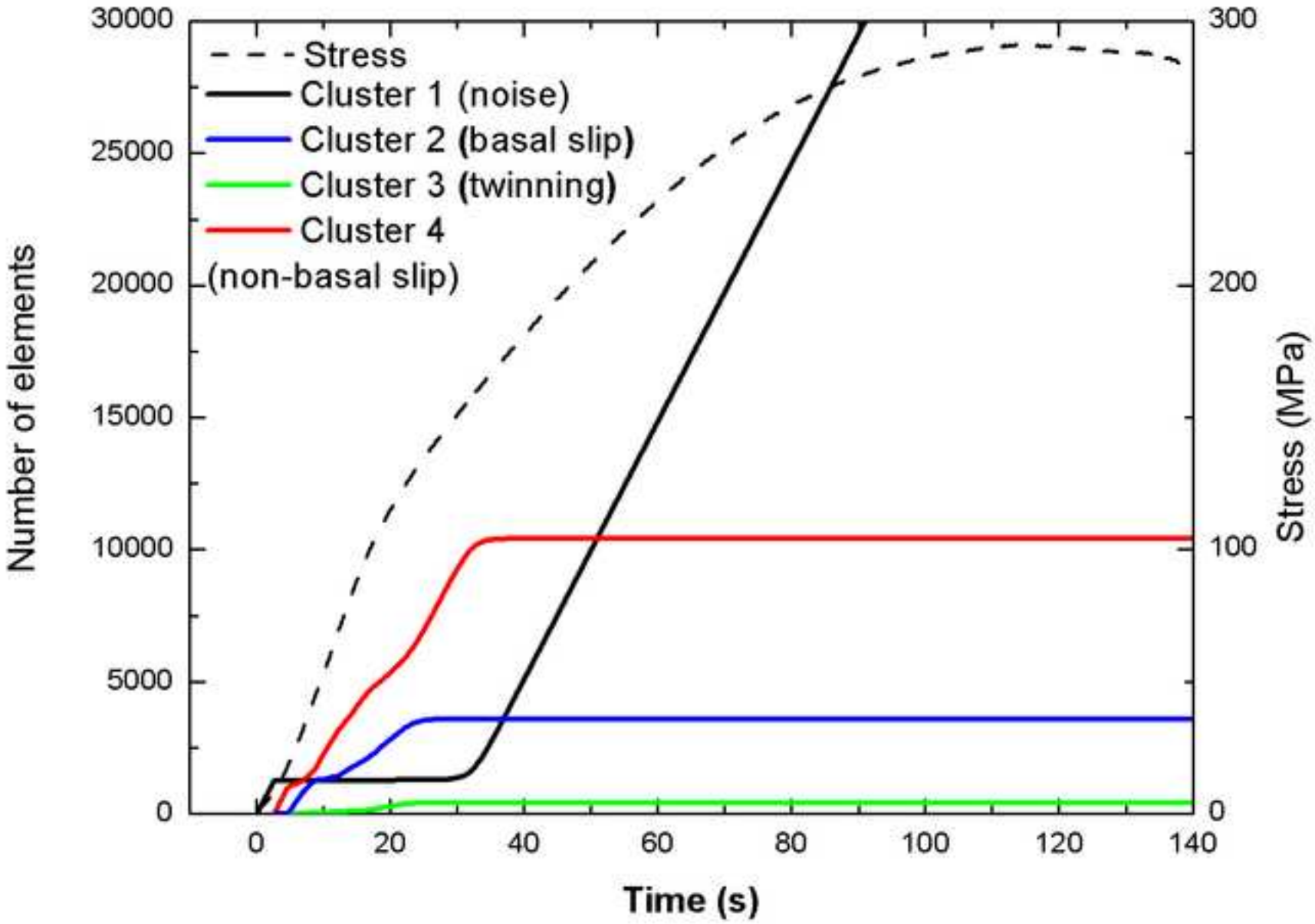

Figure 9a
Click here to download high resolution image

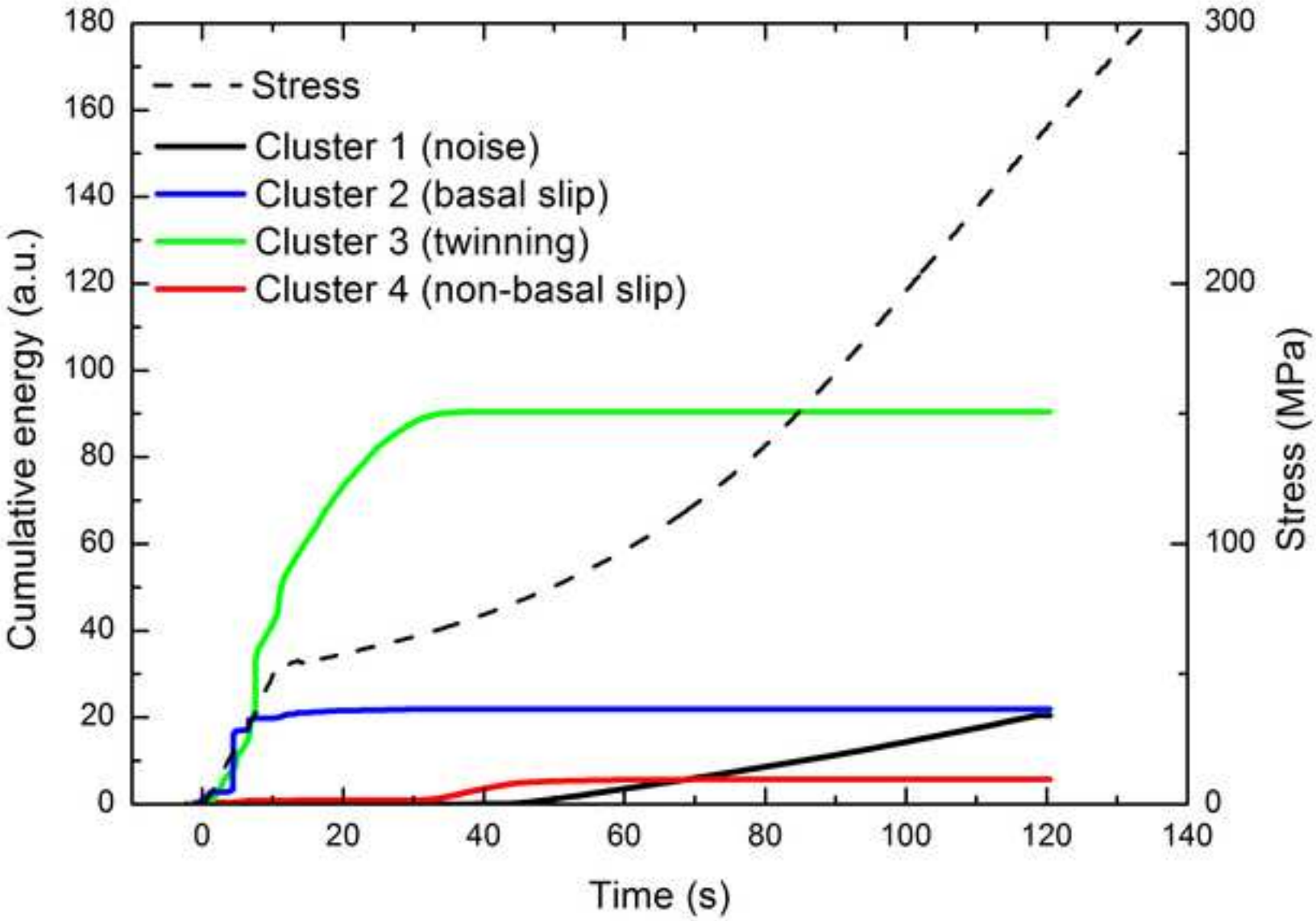

Figure 9b

Click here to download high resolution image

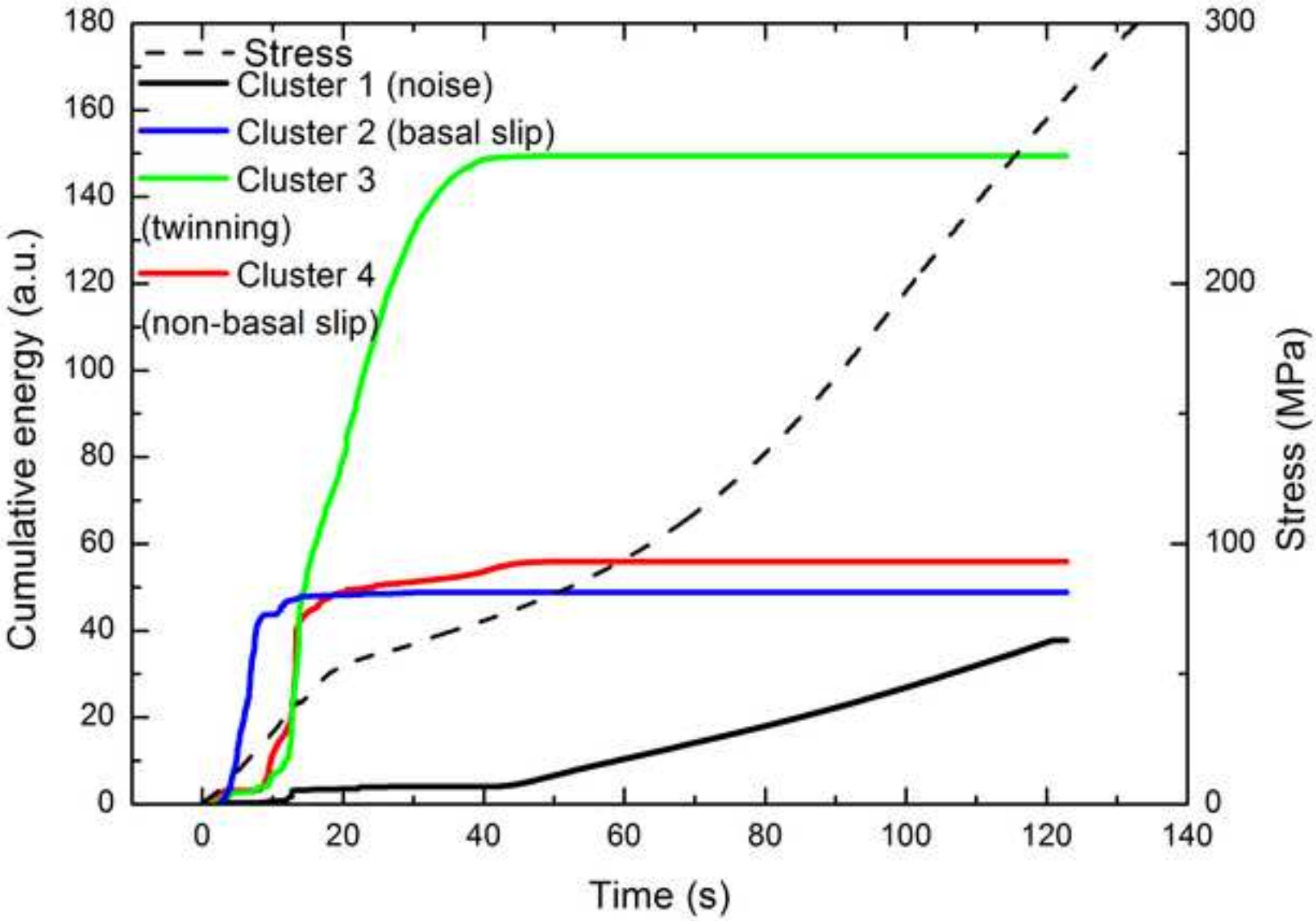

Figure 9c
Click here to download high resolution image